First Results of Differential Doppler Positioning with Unknown Starlink Satellite Signals

Mohammad Neinavaie
Department of Mechanical and Aerospace Engineering
University of California, Irvine
Irvine, CA 92697
mneinava@uci.edu

Zeinab Shadram
Department of Mechanical and Aerospace Engineering
University of California, Irvine
Irvine, CA 92697
zshadram@uci.edu

Sharbel Kozhaya
Department of Electrical Engineering and Computer Science
University of California, Irvine
Irvine, CA 92697
skozhaya@uci.edu

Zaher M. Kassas
Department of Mechanical and Aerospace Engineering
Department of Electrical Engineering and Computer Science
University of California, Irvine
Irvine, CA 92697
zkassas@ieee.org

Abstract— **This paper shows the first results of differential Doppler positioning with *unknown* low Earth orbit (LEO) Starlink satellite signals. To this end, a receiver capable of acquiring and tracking the Doppler frequency of Starlink satellites is developed. A sequential method is proposed to estimate the number of active Starlink satellites and their corresponding reference signals (RSs). The proposed method is based on the classic linear model, where it is shown that the classic linear model results in the so-called matched subspace detector. A closed form of the probability of false alarm in the presence of Doppler estimation error is derived. Next, a Doppler tracking algorithm is designed, which is based on the generalized likelihood ratio (GLR) detector. In order to compensate for the high dynamics of Starlink LEO satellites, a linear chirp model is employed in the Doppler tracking algorithm, and a Kalman filter (KF)-based tracking algorithm is designed to track the chirp parameters. To validate the proposed framework, experimental results are presented in which a base with a known position and a rover with an unknown position were equipped with the proposed receiver. Despite the unknown nature of Starlink satellite signals, it is shown that the proposed receiver is capable of acquiring three Starlink satellites and tracking their Doppler frequencies. Next, two baselines between the base and rover receivers were considered: 1 km and 9 m. Despite the fact that the satellites' ephemerides are poorly known (with errors on the order of several kilometersm since they are predicted from two-line element (TLE) files and an SGP4 propagator), the proposed differential framework was able to estimate the rover's two-dimensional position with an error of 5.6 m and 2.6 m, respectively.**

TABLE OF CONTENTS

978-1-6654-3760-8/22/$31.00 ©2022 IEEE

2022 IEEE Aerospace Conference (AERO) | 978-1-6654-3760-8/22/$31.00 ©2022 IEEE | DOI: 10.1109/AERO53065.2022.9843493

1. INTRODUCTION

Satellite-based navigation is witnessing the new era of low Earth orbit (LEO) *megaconstellations* [1]. The launch of tens of thousands of LEO satellites for broadband communications will revolutionize the future of satellite communications as well as navigation [2]. The potential of utilizing LEO space vehicle (SV) signals for navigation has been the subject of numerous recent studies [3–11]. Two main LEO-based navigation approaches have been considered in the literature: (i) tailoring the broadband protocols to support navigation capabilities [12–16] and (ii) exploiting opportunistically existing broadband LEO SV signals for navigation [17–22]. Adding navigation capabilities to LEO SVs requires significant changes to existing designs and transmission protocols and could result in charging the user an additional cost for positioning and navigation services. In contrast, broadband communication signals transmitted from LEO SVs already contain timing signals, which if one could acquire and track, navigation observables (pseudorange, carrier phase, and Doppler) could be extracted; hence, enabling positioning and navigation in an opportunistic fashion.

LEO SVs possess desirable attributes for positioning and navigation [23, 24]: (i) powerful: the received signal power is between 24 to 34 dBs higher than that of global navigation satellite systems (GNSS) SVs, which reside in medium Earth orbit (MEO); (ii) abundance: tens of thousands of broadband LEO SVs are expected to be deployed into LEO; and (iii) geometric and frequency diversity: each constellation deploys its SVs into different orbits, transmitting in a wide range of frequency bands.

Several challenges need to be addressed to exploit LEO SVs for navigation. First, the SVs' ephemerides are poorly known. While Keplerian elements parameterizing LEO SVs' orbits are made publicly available by the North American Aerospace Defense Command (NORAD) and are updated daily in the two-line element (TLE) files, using TLEs and orbit determination algorithms (e.g., SGP4) could result in a propagated satellite orbit error on the order of several kilometers. Second, broadband LEO SVs may not be necessarily equipped with atomic clocks nor are be as tightly

synchronized as GNSS SVs. Unlike GNSS, where corrections to the orbital elements and clock errors are periodically transmitted to the receiver in the navigation message, such orbital elements and clock corrections may not be available for LEO SVs [5]. Third, obtaining navigation observable using the timing signals requires knowledge of the timing signal specifications, which may not publicly disclosed. Private networks and broadband providers do not usually disclose the specification of the transmitted signal structure. For instance, very limited information about Starlink satellite signals is available [25]. Another example is the Globalstar satellite system, which supposedly uses a similar protocol to the IS-95 and cdma2000 cellular code-division multiple access (CDMA) system but with different pseudo-noise (PN) sequences [26].

In this paper, the above challenges are addressed by (i) developing a differential Doppler positioning framework to compensate for large ephemeris errors of Starlink SVs as well as the SVs' unknown clock states and (ii) developing a matched subspace detection method to estimate the unknown signals transmitted by Starlink SVs. Specifically, the contributions of this work are as follows:

- Using a general linear model, a generalized likelihood ratio (GLR) is derived, which is capable of detecting an unknown source in the presence of interfering sources. It is shown that the proposed GLR test is equivalent to a matched subspace detector. To the best of the authors' knowledge, the equivalency of the general linear model and the matched subspace detector has not been established in the published literature and is shown in this paper for the first time.
- Based on the proposed GLR test, a sequential detector is derived to detect the presence of multiple Starlink satellites on the same channel and provide an estimate of the number of active Starlink satellites. The detector relies on matched subspace detection, where the signal subspace is defined by the Doppler frequencies of the Starlink satellites. The sequential GLR detector estimates the number of Starlink satellites along with their Doppler frequencies, and it provides an initial estimate of their unknown timing signals.
- A closed-form solution of the probability of false alarm is derived in the presence of Doppler estimation error.
- Experimental results are presented showing that despite the unknown nature of Starlink satellite signals, the proposed receiver is capable of acquiring three Starlink satellites and tracking their Doppler frequencies.
- Experimental results are presented in which a base with a known position and a rover with an unknown position were equipped with the proposed receiver. Two baselines between the base and rover receivers were considered: 1 km and 9 m. Despite the fact that the satellites' ephemerides are poorly known (with errors on the order of several kilometersm since they are predicted from TLE files and an SGP4 propagator), the proposed differential framework was able to estimate the rover's two-dimensional position with an error of 5.6 m and 2.6 m, respectively.

To the authors' knowledge, the results presented in this paper are the *first* to demonstrate successful *simultaneous* acquisition and Doppler tracking of *multiple* unknown Starlink LEO SVs' signals. In addition, the positioning results achieved via the developed differential framework are the most accurate to-date (on the order of a few meters) with Starlink LEO SVs, despite the large SVs' ephemerides errors (on the order of several kilometers), arising from inaccurate TLE+SGP4 SV orbit propagation.

The remainder of this paper is organized as follows. Section 2 surveys related work in navigation with known and unknown signals of opportunity, navigation with Starlink LEO SV signals, and differential positioning. Section 3 presents the proposed baseband signal model. Section 4 discusses the proposed receiver structure to acquire and track unknown Starlink LEO signals. Section 5 formulates the proposed differential Doppler positioning framework. Section 6 presents the first experimental results of differential Doppler positioning with Starlink LEO SVs with two base/rover baseline: 1 km and 9 m. Section 7 gives concluding remarks.

2. Related Work

Opportunistic Navigation

Over the past decade, opportunistic navigation has been demonstrated in the literature with different types of signals, commonly referred to as signals of opportunity (SOPs) [27]. SOP examples include cellular [28, 29], digital television [30, 31], AM/FM [32, 33], Wi-Fi [34, 35], and low-earth orbit (LEO) satellite signals [36, 37]. Opportunistic navigation frameworks usually rely on the broadcast reference signals (RSs), which are used to derive direction-of-arrival (DOA) and time-of-arrival (TOA) [38]. These signals are known at the user equipment (UE) and are universal across network operators. Hence, they can be exploited for positioning without the need for the UE to be a network subscriber. In orthogonal frequency-division multiple access (OFDMA)-based systems, such as long-term evolution (LTE) and 5G new radio (NR) networks, several RSs, e.g., the cell-specific reference signal (CRS) and the primary and secondary synchronization signals (PSS and SSS, respectively), are broadcast at a regular and known time intervals [39–43]. While meter-level and submeter-level SOP-based navigation solutions were demonstrated on ground vehicles and UAVs, respectively, the aforementioned approaches relied on the knowledge of a subset of the RSs transmitted by the SOP [44,45]. These methods would fail if (i) the receiver enters an unknown SOP environment where the number of active SOPs and their corresponding RSs are unknown or (ii) some signal parameters change due to the dynamic nature of wireless protocols.

Navigation with Unknown Signals

The detection problem of an unknown source in the presence of other interfering signals falls into the paradigm of *matched subspace detectors* which has been widely studied in the classic detection theory literature [46, 47]. Matched subspace detectors are used frequently in radar signal processing, e.g., in source positioning in multiple-input multiple-output (MIMO) radars [48] and passive bistatic radar [49]. In [50], the design of subspace matched filters in the presence of mismatch in the steering vector was addressed. In [51], adaptive vector subspace detection in partially homogeneous Gaussian disturbance was addressed. In [52], the performance of low-rank adaptive normalized matched subspace detectors was studied. In [53], the structure of the noise covariance matrix was exploited to enhance the matched subspace detection performance. In [54], the idea of subspace matching was used to present a solution to the problem of detecting the number of signals in both white and colored noise. Recently, machine learning approaches have been proposed for unknown transmitter detection, identification, and classification [55, 56]. In the navigation literature, detection of unknown signals has been studied to design frameworks which are capable of navigating with unknown or partially known signals. The problem of detecting Galileo and Compass satel-

lites signals was studied in [57], which revealed the spread spectrum codes for these satellites. Preliminary experiments on navigation with partially known signals from low and medium Earth orbit satellites were conducted in [58–61]. In particular, a chirp parameter estimator was used in [59] to blindly estimate the GPS pseudorandom noise (PRN) codes. In [60], a blind channel estimator was proposed to exploit Orbcomm satellite signals for navigation purposes. In [61], OFDM signals were emulated from Orbcomm LEO SVs and an FFT-based Doppler estimator was proposed to exploit these signals for navigation purposes. In [62], a cognitive opportunistic navigation framework was developed. It should be pointed out that [62] considered terrestrial signals, which experience Doppler frequencies that are significantly lower than the Doppler frequencies of LEO SVs. This limits the applicability of the framework proposed in [62] to LEO SVs. This paper generalizes the framework proposed in [62] to LEO SVs by considering higher order Doppler models to compensate for the high dynamics of LEO SVs. Moreover, it is shown that the matched subspace detector, employed in [62] and other matched subspace detection algorithms (e.g. [46–49, 63]), is *equivalent* to the so-called general linear model in detection theory.

Navigation with Starlink Signals

An opportunistic framework to navigate with differential carrier phase measurements from megaconstellation LEO SV signals was proposed in [36]. The Starlink constellation is used as a specific megaconstellation example to demonstrate the efficacy of the proposed algorithm in [36].The first standalone (non-differential) positioning results with Starlink SV signals were presented in [25, 64], which show carrier phase and Doppler tracking of six Starlink SVs, achieving a horizontal positioning error of 7.7 and 10 m with known receiver altitude, respectively. To take the SV ephemeris errors into account in these papers, assuming that most of the ephemeris error is along the SV's track, the time epoch of the TLE files was shifted such that it minimizes the Doppler residuals, knowing the receiver's location. Alternatively, the ephemeris of the TLE files can be corrected online through a satellite ephemeris estimation framework, such as simultaneous tracking and navigation (STAN) [11, 65]. In this paper, SV ephemeris errors are addressed by using a differential framework. It is worth noting that the methods presented in [25,64] are not capable of estimating the number of unknown SVs if more than one Starlink SV are overhead simultaneously. In this paper, a sequential detection algorithm is developed, which is capable of estimating the number of unknown SVs in the environment. It should be pointed out that the methods presented in this paper are general enough to be applied to any LEO constellation, beyond Starlink.

Differential Navigation

Differential positioning methods assess measurement errors for each satellite using a stationary surveyed reference antenna and broadcasts error corrections to many users (which may each see a different set of satellites) [66]. Satellite errors removed by differential methods include clock calibration, ephemeris errors, ionospheric delays, and tropospheric delays [67]. A differential carrier-phase navigation system with GPS and LEO SVs was presented in [68]. The problem of navigation with differential carrier phase measurements from LEO SV megaconstellations was tackled in [36], by assuming *knowledge* of the transmitted signals. To the best of the author's knowledge, this paper presents the first differential Doppler positioning results with *unknown* Starlink satellite signals.

3. Baseband Signal Model

In most commercial communication systems, a periodic RS is transmitted, e.g., PSS in OFDMA-based and spreading codes in CDMA-based signals. In this paper, the Starlink LEO SV downlink signal is modeled as an unknown periodic signal in the presence of interference and noise. If an RS, such as PSS in OFDMA-based signals, is being periodically transmitted, it will be detected and estimated by the proposed method. The proposed signal model is

$$r[n] = \sum_{i=1}^{N} \alpha_i(\tau_n) c_i[\tau_n - t_{s_i}[n]] \exp\left(j\theta_i[\tau_n]\right) + d_i[\tau_n - t_{s_i}[n]] \exp\left(j\theta_i[\tau_n]\right) + w[n], \quad (1)$$

where $r[n]$ is the received signal at the nth time instant; $\alpha_i(\tau_n)$ is the complex channel gain between the receiver and the ith Starlink LEO satellite vehicle (SV); τ_n is the sample time expressed in the receiver time; $c_i[n]$ represents the samples of the complex periodic RS with a period of L samples; $t_{s_i}[n]$ is the code-delay corresponding to the receiver and the ith Starlink LEO SV at the nth time instant; $\theta_i[\tau_n] = 2\pi f_{D_i}[n] T_s n$ is the carrier phase in radians, where $f_{D_i}[n]$ is the instantaneous Doppler frequency at the nth time instant and T_s is the sampling time; $d_i[\tau_n]$ represents the complex samples of some data transmitted from the ith Starlink LEO SV; and $w[n]$ is a complex zero-mean independent and identically distributed noise with variance σ_w^2.

Starlink LEO SV's signals suffer from very high Doppler shifts. Higher lengths of processing intervals require higher order Doppler models. In order for a Doppler estimation algorithm to provide an accurate estimation of the Doppler frequency, the processing interval should be large enough to accumulate enough energy. According to the considered processing interval length in the experiments, it is observed that during the kth processing interval, the instantaneous Doppler frequency is almost a linear function of time, i.e.,

$$f_{D_i}[n] = f_{D_{k,i}} + \beta_{k,i} n, \quad k = 0, \ldots, K, \quad (2)$$

where $f_{D_{k,i}}$ is referred to as constant Doppler, $\beta_{k,i}$ is the Doppler rate at the kth processing interval corresponding to the ith Starlink SV, and K is the total number of processing intervals.

Definition: The coherent processing interval (CPI) is defined as the time interval in which the channel gain $\alpha_i(\tau_n)$, Doppler $f_{D_{k,i}}$ and the Doppler rate $\beta_{k,i}$, are all constant. Since it is assumed that the channel gain is constant during one CPI, it is assumed that the channel gain is a function of the CPI index, i.e., $\alpha_i(\tau_n) = \alpha_{i,k}$, where n is in the kth CPI.

The received signal at the nth time instant when the Doppler rate is wiped-off is denoted by $r'[n] \triangleq \exp(-j2\pi\beta_{k,i}n^2) r[n]$. One can define

$$s_{k,i}[n] \triangleq \alpha_{i,k} c[\tau_n - t_{s_i}[n]] \exp\left(j2\pi f_{D_{i,k}} T_s n\right), \quad (3)$$

and the equivalent noise as

$$w_{\mathrm{eq}_{k,i}}[n] = d[\tau_n - t_{s_i}[n]] \exp\left(j2\pi f_{D_{k,i}} T_s n\right) + \exp\left(-j2\pi\beta_{k,i}n^2\right) w[n]. \quad (4)$$

Hence,

$$r'[n] = \sum_{i=1}^{N} \left(s_{k,i}[n] + w_{\mathrm{eq}_{k,i}}[n] \right). \quad (5)$$

Due to the periodicity of the RS, $s_{k,i}[n]$ has the following property

$$s_{k,i}[n+mL] = s_{k,i}[n]\exp\left(j\omega_{k,i}mL\right) \quad 0 \le n \le L-1, \tag{6}$$

where $\omega_{k,i} = 2\pi f_{D_{k,i}} T_s$ is the normalized Doppler at the kth CPI, corresponding to the ith Starlik SV, and $-\pi \le \omega_{k,i} \le \pi$. A vector of L observation samples corresponding to the mth period of the signal is formed as

$$\mathbf{z}_m \triangleq [r'[mL], r'[mL+1], \ldots, r'[(m+1)L-1]]^{\mathsf{T}}. \tag{7}$$

The kth CPI vector is constructed by concatenating M vectors of length L to form the $ML \times 1$ vector

$$\mathbf{y}_k = [\mathbf{z}_{kM}^{\mathsf{T}}, \mathbf{z}_{kM+1}^{\mathsf{T}}, \ldots, \mathbf{z}_{(k+1)M-1}^{\mathsf{T}}]^{\mathsf{T}}. \tag{8}$$

Therefore,

$$\mathbf{y}_k = \mathbf{h}_{k,i}\mathbf{s}_{k,i} + \mathbf{w}_{\mathrm{eq}_k}, \tag{9}$$

where $\mathbf{s}_{k,i} = [s_{k,i}[1], s_{k,i}[2], \ldots, s_{k,i}[L]]^{\mathsf{T}}$, and the $ML \times L$ Doppler matrix is defined as

$$\mathbf{h}_{k,i} \triangleq [\mathbf{I}_L, \exp\left(j\omega_{k,i}L\right)\mathbf{I}_L, \ldots, \exp\left(j\omega_{k,i}(M-1)L\right)\mathbf{I}_L]^{\mathsf{T}}, \tag{10}$$

where $\mathbf{I}_L$ is an $L \times L$ identity matrix, and $\mathbf{w}_{\mathrm{eq}_k}$ is the equivalent noise vector.

4. RECEIVER STRUCTURE

This section presents the structure of the proposed receiver. The proposed receiver consists of two main stages: (i) acquisition and (ii) tracking. Each of these stages is discussed in detail next.

Acquisition

In this paper, the acquisition stage is modeled as a sequential matched subspace detection problem. The acquisition stage is performed in the first CPI, i.e., $k = 1$. Therefore, to simplify notation in the acquisition stage, the k index is dropped. The acquisition stage comprises estimating the number of LEO SVs, the period of the RS, an initial estimate of normalized Doppler along with the Doppler rate, and the RSs, i.e., N, L, ω_i, β_i, and $\mathbf{s}_i$, respectively. At each step of the acquisition, a test is performed to detect the most powerful Starlink LEO SV signal when the subspace of the previously detected Starlink LEO SVs are nulled. In the following subsection, matched subspace detection is overviewed and the hypothesis test for detection of multiple Starlink LEO SVs is formulated.

Matched Subspace Detector—As mentioned previously, in the first step of the proposed sequential algorithm, the presence of a single Starlink LEO SV is tested and if the null hypothesis is accepted, then $\hat{N} \equiv 0$, which means that no Starlink LEO SV is detected to be present in the environment under the test. If the test rejects the null hypothesis, the algorithm verifies the presence of at least one source and performs the test to detect the presence of other Starlink LEO SVs in the presence of the previously detected Starlink LEO SVs. The unknown Doppler and the RS of each Starlink LEO SVs are estimated at each step. In general, if the null hypothesis at the ith level of the sequential algorithm is accepted, the algorithm is terminated and the estimated number of LEO SVs will be $\hat{N} = i - 1$. It should be noted that one could obtain from the TLE files a nominal value β_0 for the Doppler rate β_i of Starlink LEO SVs, which is the minimum possible Doppler rate for Starlink satellites or any other constellation of interest. Hence, at each step of the algorithm, if the Doppler rate, i.e., β_i, of the detected source is less than β_0, the detected source will be excluded from the acquired sources.

In order to test the presence of $\mathbf{s}_i$, at the ith stage of the acquisition algorithm, the observation vector can be written as

$$\mathbf{y} = \mathbf{H}_i\mathbf{s}_i + \mathbf{B}_{i-1}\boldsymbol{\theta}_{i-1} + \mathbf{w}_{\mathrm{eq}_i}, \tag{11}$$

$$\mathbf{B}_{i-1} \triangleq [\mathbf{H}_1, \mathbf{H}_2, \ldots, \mathbf{H}_{i-1}],\ \boldsymbol{\theta}_{i-1} \triangleq [\mathbf{s}_1^{\mathsf{T}}, \mathbf{s}_2^{\mathsf{T}}, \ldots, \mathbf{s}_{i-1}^{\mathsf{T}}]^{\mathsf{T}}. \tag{12}$$

The following binary hypothesis test is used to detect the ith Starlink SV:

$$\begin{cases} \mathcal{H}_0^i: & \mathbf{A}\boldsymbol{\theta}_i = \mathbf{0} \\ \mathcal{H}_1^i: & \mathbf{A}\boldsymbol{\theta}_i \neq \mathbf{0}. \end{cases} \tag{13}$$

Where, $\mathbf{A} = [\mathbf{I}_L, \mathbf{0}, \ldots, \mathbf{0}]$ is an $L \times iL$ matrix.

Theorem 1: For a given set of Doppler frequencies, Doppler rates, and period, i.e., $\mathcal{W}_i = \{L, \omega_1, \beta_1, \omega_2, \beta_2, \ldots, \omega_i, \beta_i\}$, the GLR at the ith stage is derived as (see Appendix A)

$$\mathcal{L}(\mathbf{y}|\mathcal{W}_i) = \frac{\|\mathbf{H}_i^{\mathsf{H}}\mathbf{P}^{\perp}_{\mathbf{B}_{i-1}}\mathbf{y}\|^2}{\|\mathbf{P}^{\perp}_{\mathbf{B}_{i-1}}\mathbf{y}\|^2} \underset{\mathcal{H}_0^i}{\overset{\mathcal{H}_1^i}{\gtrless}} \eta_i, \tag{14}$$

where $\mathbf{y}^{\mathsf{H}}$ is the Hermitian transpose of $\mathbf{y}$, $\mathbf{P}_{\mathbf{X}} \triangleq \mathbf{X}(\mathbf{X}^{\mathsf{H}}\mathbf{X})^{-1}\mathbf{X}^{\mathsf{H}}$ denotes the projection matrix to the column space of $\mathbf{X}$, and

$$\mathbf{P}^{\perp}_{\mathbf{X}} \triangleq \mathbf{I}_L - \mathbf{X}\left(\mathbf{X}^{\mathsf{H}}\mathbf{X}\right)\mathbf{X}^{\mathsf{H}}, \tag{15}$$

denotes the projection matrix onto the space orthogonal to the column space of $\mathbf{X}$.

If the subspace spanned by the columns of $\mathbf{P}^{\perp}_{\mathbf{B}_{i-1}}\mathbf{H}_i$, is viewed as the *ith Starlink LEO SV's signal subspace*, and the orthogonal subspace as the *noise subspace*, then the likelihood (14) can be interpreted as an estimated signal to noise ratio (SNR). The reader is referred to [46] for further interpretations of matched subspace detectors.

In this paper, the period of all the RSs are assumed to be equal. Hence, searching over the period is performed once. At the ith stage of the proposed sequential algorithm, the GLR requires an estimate of the set $\mathcal{W}_i$. The sequential nature of the algorithm enables separate estimation of the Doppler frequency at each step. For instance, at the first step of the algorithm, a two-dimensional search is required to obtain the maximum likelihood (ML) estimate of ω_1 and β_1, denoted by $\hat{\omega}_1$ and $\hat{\beta}_1$, respectively. In the second stage of the algorithm, $\hat{\omega}_1$ and $\hat{\beta}_1$ are used to construct the projection matrix to null the subspace of the first Starlink SV. Consequently, at the ith step of the algorithm, invoking the previously estimated Dopplers, a two-dimensional search is required to estimate ω_i and β_i, and construct the estimated projection matrix and the estimated Doppler matrix for the corresponding stage, denoted by $\hat{\mathbf{P}}_{\mathbf{S_i}}$ and $\hat{\mathbf{H}}_i$, respectively.

Therfore, by replacing the ML estimate of the elements of $\mathcal{W}_i$, the GLR can be written as

$$\mathcal{L}(\mathbf{y}) = \frac{\|\hat{\mathbf{H}}_i^{\mathsf{H}}\hat{\mathbf{P}}^{\perp}_{\hat{\mathbf{B}}_{i-1}}\mathbf{y}\|^2}{\|\hat{\mathbf{P}}^{\perp}_{\hat{\mathbf{B}}_{i-1}}\mathbf{y}\|^2} \underset{\mathcal{H}_0^i}{\overset{\mathcal{H}_1^i}{\gtrless}} \eta_i. \tag{16}$$

where η_i is a predetermined threshold at the ith stage using the probability of false alarm which will be discussed later in this subsection. The ML estimate of ω_i and β_i, are obtained by maximizing the likelihood function under $\mathcal{H}_1^i$ which yields

$$\hat{\omega}_i = \arg\max_{\omega_i,\beta_i} \|\mathbf{H}_i^{\mathsf{H}} \mathbf{P}^{\perp}_{\mathbf{B}_{i-1}} \mathbf{y}\|^2, \tag{17}$$

and is used to construct $\hat{\mathbf{P}}_{\mathbf{B}_{i-1}}$ and $\hat{\mathbf{H}}_i$.

It should be pointed out that according to (52) in Appendix A,

$$\mathbf{H}_i^{\mathsf{H}} \mathbf{P}^{\perp}_{\mathbf{B}_{i-1}} \mathbf{H}_i = \lambda_i \mathbf{I}_L, \tag{18}$$

where the scalar λ_i is the Schur complement of block $\mathbf{C_{i-1}}$, where

$$\mathbf{C}_i = \begin{bmatrix} c_{11} & c_{12} & \dots & c_{1i} \\ c_{21} & c_{22} & \dots & c_{2i} \\ \vdots & \ddots & \ddots & \vdots \\ c_{i1} & c_{i2} & \dots & c_{ii} \end{bmatrix}. \tag{19}$$

For a known $\mathcal{W}_i$, the least squares (LS) estimate of the ith source, i.e., $\mathbf{s}_i$, is given by

$$\hat{\mathbf{s}}_i = \frac{1}{\lambda_i} \mathbf{H}_i^{\mathsf{H}} \mathbf{P}^{\perp}_{\mathbf{B}_{i-1}} \mathbf{y}. \tag{20}$$

It should be noted that the estimated RS, i.e., $\hat{\mathbf{s}}_i$, contains the effect of the channel between the Starlink LEO SV and the UE. Small values of $|\alpha_i|$ degrades the estimation quality of the desired RS and, consequently, affects the acquisition and tracking performance. It should also be pointed out that $\frac{1}{\lambda_i}\mathbf{H}_i^{\mathsf{H}} \mathbf{P}^{\perp}_{\mathbf{B}_{i-1}} \mathbf{y} = \mathbf{s}_i + \mathbf{w}_{\mathrm{acq}_i}$, where $\mathbf{w}_{\mathrm{acq}_i} = \frac{1}{\lambda_i}\mathbf{H}_i^{\mathsf{H}} \mathbf{P}^{\perp}_{\mathbf{B}_{i-1}} \mathbf{w}_{\mathrm{eq}_i}$. In other words, for a known Doppler frequency, the LS estimator of the ith source is an unbiased estimator, i.e., $\mathbb{E}\{\hat{\mathbf{s}}_i\} = \mathbf{s}_i$. However, since the true Doppler is not known to the receiver, the ML estimate of the Doppler is used to compute the LS estimate of the ith RS instead. Moreover, using (18), it can be shown that

$$\frac{1}{\hat{\lambda}_i} \hat{\mathbf{H}}_i^{\mathsf{H}} \hat{\mathbf{P}}_{\mathbf{B}_{i-1}} \mathbf{H}_i = \beta_{\mathrm{acq}_i} \mathbf{I}_L, \tag{21}$$

where β_{acq_i} is some complex scalar. As such, the LS estimate of the RS using the ML estimate of the Doppler becomes

$$\hat{\mathbf{s}}_i = \frac{1}{\hat{\lambda}_i} \hat{\mathbf{H}}_i^{\mathsf{H}} \hat{\mathbf{P}}^{\perp}_{\mathbf{B}_{i-1}} \mathbf{y} = \beta_{\mathrm{acq}_i} \mathbf{s}_i + \hat{\mathbf{w}}_{\mathrm{acq}_i}, \tag{22}$$

where $\hat{\mathbf{w}}_{\mathrm{acq}_i} \triangleq \frac{1}{\hat{\lambda}_i} \hat{\mathbf{H}}_i^{\mathsf{H}} \hat{\mathbf{P}}^{\perp}_{\mathbf{B}_{i-1}} \mathbf{w}_{\mathrm{eq}_i}$. Furthermore, the asymptotic efficiency property of the ML estimator results in $|\beta_{\mathrm{acq}_i}| \to 1$ as $K \to \infty$ [69].

Remark: Since for the constellation of interest $\beta_i \leq \beta_0$, in the sequential detection algorithm, the detected sources with smaller Doppler rate than β_0 are excluded from the detected sources.

Probability of False Alarm—The Doppler estimation error affects the probability of detection and the probability of false alarm. For known subspaces and the corresponding projection matrices, using Theorem 7.1 in [70], one can show that the probability of false alarm for the ith stage of the likelihood in (14) asymptotically tends to

$$P_{\mathrm{fa}_i} = \exp\left(-L\eta_i\right) \sum_{n=0}^{L-1} \frac{(L\eta_i)^n}{n!}, \tag{23}$$

for a large number of observation samples. In other words, the detector is not a function of unknown parameters when the matrix $\mathbf{H}_i$ is known at the receiver, which ensures the constant false alarm rate (CFAR) property. However, in a practice, $\mathbf{H}_i$ is unknown and the Doppler frequency is estimated which introduces a Doppler estimation error. In the following theorem, it is shown that in the presence of Doppler estimation error, the CFAR property is guaranteed under certain circumstances. Theroemt 2 provides a closed form solution for the probability of false alarm in the presence of Doppler estimation error.

Theorem 2: Consider two Starlink LEO SVs with Doppler frequencies ω_1 and ω_2 and corresponding estimates $\hat{\omega}_1$ and $\hat{\omega}_2$, respectively. Define the Doppler estimation error of ω_1 as $\Delta\omega_1 \triangleq \omega_1 - \hat{\omega}_1$. As $K \to \infty$, the probability of false alarm equals

$$P_{\mathrm{fa}_i} = \exp\left(-L\eta_i\right) \sum_{n=0}^{L-1} \frac{(L\eta_i)^n}{n!}, \tag{24}$$

with probability one, if (i) $|\Delta\omega_1 L| \ll \frac{1}{K}$ and (ii) $|\hat{\omega}_2 L - \hat{\omega}_1 L| > \frac{1}{K}$.

Proof: See Appendix B.

Theorem 2 specifies the *resolution* of the Detection algorithm in terms of Doppler frequency. More precisely, it is observed that if the difference between the Doppler frequencies of two Starlink LEO SVs is larger than the reciprocal of the CPI, the detector follows the CFAR property. While the CFAR property of the matched subspace detector is guaranteed for known Doppler frequencies, Theorem 2 specifies the sufficient conditions to ensure the CFAR property in the presence of Doppler estimation error. The acquisition algorithm is summarized in Algorithm 1.

Algorithm 1 Sequential Matched Subspace Detector

Input: $\mathbf{y}$, P_{fa}
Output: $\hat{N}$, $\hat{\omega}_i$, and $\hat{\mathbf{s}}_i$ for $i = 1, \dots, \hat{N}$
1: Initialization: $i = 1$, $j = 0$, $\mathbf{P}^{\perp}_{\mathbf{B}_0} = \mathbf{I}_L$
2: Calculate $\mathcal{L}_i(\mathbf{y})$ according to (16) and the threshold using (61).
3: **if** $\mathcal{L}_i(\mathbf{y}) < \eta_i$, **then**
4: $\quad \hat{N} = i - 1 - j$.
5: $\quad$ Break
6: Estimate ω_i, β_i according to (17), and construct $\hat{\mathbf{H}}_i$, $\hat{\mathbf{P}}^{\perp}_{\mathbf{B}_{i-1}}$, and $\hat{\lambda}_i$ using (52)
7: $\hat{\mathbf{s}}_i = \frac{1}{\hat{\lambda}_i} \hat{\mathbf{H}}_i^{\mathsf{H}} \hat{\mathbf{P}}^{\perp}_{\mathbf{B}_{i-1}} \mathbf{y}$
8: **if** $\beta_i < \beta_0$ **then**
9: $\quad j = j + 1$.
10: $i \leftarrow i + 1$, update $\hat{\mathbf{P}}^{\perp}_{\mathbf{B}_{i-1}}$ using $\hat{\omega}_i$, and go to step 2.

Kalman Filter-Based Doppler Tracking

The time-varying component of the continuous-time true Doppler is a function of (i) the true range rate between the LEO SV and the receiver, denoted by $\dot{d}(t)$ and (ii) the time-varying difference between the receiver's and LEO SV's clock bias rate, denoted by $\dot{b}(t)$ and expressed in meters per second. Hence,

$$\omega(t) = 2\pi \left[-\frac{\dot{d}(t)}{\lambda} + \frac{\dot{b}(t)}{\lambda} + f_a \right], \tag{25}$$

where λ is the carrier wavelength. The clock bias is assumed to have a constant drift, i.e., $b(t) = a(t - t_0) + b_0$. Moreover, simulations with Starlink LEO SVs show that the following kinematic model for $d(t)$ holds for short period of times

$$\dddot{d}(t) = \tilde{w}(t), \tag{26}$$

where $\tilde{w}$ is a zero-mean white noise process with power spectral density $q_{\tilde{w}}$. Let k denote the time index corresponding to $t_k = kT + t_0$, where $T = M \cdot L \cdot T_s$ is the sampling interval, also known as subaccumulation period, and $M \cdot L$ is the number of subaccumulated samples. The discrete-time kinematic model of the Doppler state vector $\boldsymbol{\omega}_k \triangleq [\omega_k, \dot{\omega}_k]^{\mathsf{T}}$ is given by

$$\boldsymbol{\omega}_{k+1} = \mathbf{F}\boldsymbol{\omega}_k + \mathbf{w}_k, \tag{27}$$

$$\mathbf{F} \triangleq \begin{bmatrix} 1 & T \\ 0 & 1 \end{bmatrix}, \quad \mathbf{Q} \triangleq q_{\tilde{w}} \begin{bmatrix} \frac{T^3}{3} & \frac{T^2}{2} \\ \frac{T^2}{2} & T \end{bmatrix}, \tag{28}$$

where $\mathbf{F}$ is the discrete-time state transition matrix, $\mathbf{w}_k$ is the discrete-time process noise with zero mean and covariance matrix $\mathbf{Q}$. The initial state is given by $\boldsymbol{\omega}_0 = \left[2\pi f_a + \frac{2\pi}{\lambda}(a - \dot{d}(t_0)), -\frac{2\pi}{\lambda}\ddot{d}(t_0)\right]^{\mathsf{T}}$.

Let $\hat{\boldsymbol{\omega}}_{k|l}$ denote the KF estimate of $\boldsymbol{\omega}_k$ given all the measurements up to time-step $l \leq k$, and $\tilde{\mathbf{P}}_{k|l}$ denote the corresponding estimation error covariance. The initial estimate $\hat{\boldsymbol{\omega}}_{0|0}$ with a corresponding $\tilde{\mathbf{P}}_{0|0}$ are provided from the acquisition stage. The KF-based tracking algorithm time update and the measurement update are discussed next.

Kalman Filter Time Update—The KF time update equations are straightforwardly given by

$$\hat{\boldsymbol{\omega}}_{k+1|k} = \mathbf{F}\hat{\boldsymbol{\omega}}_{k|k}, \tag{29}$$

$$\tilde{\mathbf{P}}_{k+1|k} = \mathbf{F}\tilde{\mathbf{P}}_{k|k}\mathbf{F}^{\mathsf{T}} + \mathbf{Q}. \tag{30}$$

Kalman Filter Measurement Update—The KF measurement update equations is carried out based on the ML estimate of the Doppler. The Doppler wipe-off is performed as $\tilde{r}_k[i] = r[i + kML] \exp\left[-j\hat{\theta}_{k+i|k}\right]$, where $\hat{\theta}_{k+i|k}$ is obtained according to $\hat{\theta}_{k+i|k} = \hat{\omega}_{k|k} i T_s + \hat{\dot{\omega}}_{k|k} \frac{i^2}{2} T_s^2$, for $i = 0, \ldots, ML - 1$. The vector $\tilde{\mathbf{y}}_{k+1}$ is constructed as $\tilde{\mathbf{y}}_{k+1} = [\tilde{r}_k[0], \tilde{r}_k[2], \ldots, \tilde{r}_k[ML-1]]^{\mathsf{T}}$. Similar to (9), one can show that

$$\tilde{\mathbf{y}}_{k+1} = \tilde{\mathbf{H}}_{k+1}\mathbf{s} + \tilde{\mathbf{w}}_{\mathrm{eq}_{k+1}}, \tag{31}$$

where the residual Doppler matrix is

$$\tilde{\mathbf{H}}_{k+1} \triangleq [\mathbf{I}_L, \exp(j\Delta\omega_k L)\mathbf{I}_L, \ldots, \exp(j\Delta\omega_{k+1}(M-1)L)\mathbf{I}_L]^{\mathsf{T}}, \tag{32}$$

and $\Delta\omega_{k+1} = \omega_{k+1} - \hat{\omega}_{k+1|k}$. The proposed KF innovation is given by

$$\nu_{k+1} = \mathrm{argmax}_{\Delta\omega_{k+1}} \frac{1}{M} \|\tilde{\mathbf{H}}_{k+1}^{\mathsf{H}} \tilde{\mathbf{y}}_{k+1}\|^2, \tag{33}$$

which is a direct measure of the Doppler error.

Kalman Filter Initialization— The initial estimates of the Doppler $\hat{\omega}_{0|0}$ and the Doppler rate $\hat{\dot{\omega}}_{0|0}$ are obtained from the acquisition stage. Let Δf_D and $\Delta \dot{f}_D$ denote the sizes of the Doppler and Doppler rate search bins. It is assumed that the initial Doppler and Doppler rate errors are uniformly distributed within one bin, and their initial probability density functions (pdfs) are bounded by Gaussian pdfs with zero-mean and standard deviations $\frac{\Delta f_D}{3}$ and $\frac{\Delta \dot{f}_D}{3}$, respectively. Therefore, the KF is initialized with

$$\hat{\boldsymbol{\omega}}_{0|0} = \left[2\pi\hat{f}_D(0), 2\pi\hat{\dot{f}}_D(0)\right]^{\mathsf{T}},$$
$$\tilde{\mathbf{P}}_{0|0} = \mathrm{diag}\left[\frac{4\pi^2}{9}\Delta f_D^2, \frac{4\pi^2}{9}\Delta \dot{f}_D^2\right]. \tag{34}$$

5. DIFFERENTIAL DOPPLER POSITIONING FRAMEWORK

In non-differential Doppler positioning, pseudorange rate observables are formed from the tracked Doppler frequencies that are multiplied by the wavelength. For the ith Starlink LEO SV, the pseudorange rate observable at time-step κ, which represents the discrete time at $t_\kappa = t_0 + \kappa T$ for an initial time t_0 and sampling time T, expressed in meters, is modeled as

$$\begin{aligned} z_{i_r}(\kappa) =& -c\frac{f_{D_{i_r}}(\kappa)}{F_c} \\ =& -\frac{\dot{\boldsymbol{r}}_{\mathrm{SV}_i}^{\mathsf{T}}(\kappa')\left[\boldsymbol{r}_r - \boldsymbol{r}_{\mathrm{SV}_i}(\kappa')\right]}{\|\boldsymbol{r}_r - \boldsymbol{r}_{\mathrm{SV}_i}(\kappa')\|} + a_{i_r} \\ &+ c \cdot \left[\delta\dot{t}_r(\kappa) - \delta\dot{t}_{\mathrm{SV}_i}(\kappa')\right] \\ &+ c\delta\dot{t}_{iono_r}(\kappa) + c\delta\dot{t}_{tropo_r}(\kappa) + v_{z_{i_r}}(\kappa), \end{aligned} \tag{35}$$

where, F_c is the carrier frequency, κ' represents discrete-time at $t_\kappa = t_0 + \kappa T - \delta t_{\mathrm{TOF}_i}$, with $\delta t_{\mathrm{TOF}_i}$ being the true time of flight of the signal from the ith Starlink LEO SV, $\boldsymbol{r}_r$ and $\boldsymbol{r}_{\mathrm{SV_i}}(\kappa)$ are the receiver's and ith Starlink LEO SV three-dimensional (3-D) position vectors, a_{i_r} is the Doppler ambiguity at the rover, and $\dot{\boldsymbol{r}}_{\mathrm{SV_i}}(\kappa)$ is the ith Starlink LEO SV 3-D velocity vector. In what follows, the effect of time of flight in the Starlink LEO SV position is neglected, i.e., $\boldsymbol{r}_{\mathrm{SV}_i}(\kappa') \approx \boldsymbol{r}_{\mathrm{SV}_i}(\kappa)$. This approximation introduces an error in the Starlink LEO SV position which is approximately common between the base and the rover. It should also pointed out that the error introduced by this approximation is of the order of couple of meters which is negligible compared to the position error in the TLE files which can be as high as few kilometers. Starlink LEO SVs' positions can be estimated through TLE files and orbit determination algorithms (e.g., SGP4 [71–73]). The parameter a_{i_r} is the constant bias due to the unknown Doppler frequency ambiguity f_a, which is introduced since the exact carrier frequency is unknown, c is the speed of light, $\delta\dot{t}_r$ and $\delta\dot{t}_{\mathrm{SV_i}}$ are the clock drifts for receiver and ith Starlink SV, respectively. Assuming a first-order clock model for both receiver and SV [74], the clock drift can be considered as constants. The ionospheric and tropospheric clock drifts are modeled as $c\delta\dot{t}_{iono}$ and $c\delta\dot{t}_{tropo}$, respectively. Additionally, $v_{z_i}(\kappa)$ is the measurement noise, which is modeled as a zero-mean, white Gaussian random sequence with variance $\sigma_i^2(\kappa)$. The value of $\sigma_i^2(\kappa)$ is the first diagonal element of $\tilde{\mathbf{P}}_{\kappa|\kappa}$, expressed in $\mathrm{m}^2/\mathrm{s}^2$.

In differential Doppler positioning, in addition to the receiver

whose position is to be estimated (the rover), one has access to Doppler measurements from the same Starlink LEO SV at another receiver (the base) whose position is known. Essentially, this framework consists of a rover receiver (r) and a base receiver (b) in an environment comprising M visible Starlink LEO SVs. The objective is to estimate the position of the rover receiver, given knowledge about the base's position and Doppler observables produced by the base on the same Starlink LEO SVs. Similar to (35), for the ith Starlink LEO SV, the pseudorange rate observable for the base at time-step κ, can be modeled as

$$\begin{aligned} z_{i_b}(\kappa) &= -c\frac{f_{D_{i_b}}(\kappa)}{F_c} \\ &= -\frac{\dot{\boldsymbol{r}}_{\mathrm{SV_i}}^{\mathsf{T}}(\kappa)\left[\boldsymbol{r}_b - \boldsymbol{r}_{\mathrm{SV_i}}(\kappa)\right]}{\|\boldsymbol{r}_b - \boldsymbol{r}_{\mathrm{SV_i}}(\kappa)\|} + a_{i_b} + c(\delta\dot{t}_b - \delta\dot{t}_{\mathrm{SV_i}}) \\ &\quad + c\delta\dot{t}_{iono_b}(\kappa) + c\delta\dot{t}_{tropo_b}(\kappa) + v_{z_{i_b}}(\kappa). \end{aligned} \tag{36}$$

By subtracting the tracked Doppler frequencies measured at the base from what is measured at the rover, the common terms, which are the satellite clock drifts will be vanished which leads to less number of unknown terms that need to be estimated. For the differential Doppler positioning framework, the measurement for the ith Starlink LEO SV can be defined by subtracting the pseudorange rate observables at the base and the rover and adding a known term as

$$\begin{aligned} \tilde{z}_{i_{r,b}}(\kappa) &= z_{i_r}(\kappa) - z_{i_b}(\kappa) + \frac{-\dot{\boldsymbol{r}}_{\mathrm{SV_i}}^{\mathsf{T}}(\kappa)\left[\boldsymbol{r}_b - \boldsymbol{r}_{\mathrm{SV_i}}(\kappa)\right]}{\|\boldsymbol{r}_b - \boldsymbol{r}_{\mathrm{SV_i}}(\kappa)\|} \\ &= -\frac{\dot{\boldsymbol{r}}_{\mathrm{SV_i}}^{\mathsf{T}}(\kappa)\left[\boldsymbol{r}_r - \boldsymbol{r}_{\mathrm{SV_i}}(\kappa)\right]}{\|\boldsymbol{r}_r - \boldsymbol{r}_{\mathrm{SV_i}}(\kappa)\|} + (a_{i_r} - a_{i_b}) \\ &\quad + c\cdot(\delta\dot{t}_r - \delta\dot{t}_b) + c\cdot\left[\delta\dot{t}_{iono_r}(\kappa) - \delta\dot{t}_{iono_b}(\kappa)\right] \\ &\quad + c\cdot\left[\delta\dot{t}_{tropo_r}(\kappa) - \delta\dot{t}_{tropo_b}(\kappa)\right] + v_{\tilde{z}_{i_{r,b}}}(\kappa). \end{aligned} \tag{37}$$

It can be assumed that the difference between ionospheric and tropospheric drifts at the base and rover are negligible, which is reasonable when the base and the rover are relatively close to each other (e.g., a few kilometers apart). The ambiguity at both the base a_{i_b} and rover a_{i_r} can be resolved by analyzing the Doppler profile for each SV. The covariance of the new measurement noise is the summation of the measurement noise covariance at base and rover. Therefore, the final differential Doppler poisoning measurement model for the ith Starlink LEO SV is obtained as

$$\tilde{z}_{i_{r,b}}(\kappa) = -c\frac{\left[f_{D_{i_r}}(\kappa) - f_{D_{i_b}}(\kappa)\right]}{F_c} \tag{38}$$

$$\begin{aligned} &+ \frac{-\dot{\boldsymbol{r}}_{\mathrm{SV_i}}^{\mathsf{T}}(\kappa)\left[\boldsymbol{r}_b - \boldsymbol{r}_{\mathrm{SV_i}}(\kappa)\right]}{\|\boldsymbol{r}_b - \boldsymbol{r}_{\mathrm{SV_i}}(\kappa)\|} \\ &= \frac{-\dot{\boldsymbol{r}}_{\mathrm{SV_i}}^{\mathsf{T}}(\kappa)\left[\boldsymbol{r}_r - \boldsymbol{r}_{\mathrm{SV_i}}(\kappa)\right]}{\|\boldsymbol{r}_r - \boldsymbol{r}_{\mathrm{SV_i}}(\kappa)\|} \\ &\quad + c\cdot(\delta\dot{t}_r - \delta\dot{t}_b) + v_{\tilde{z}_{i_{r,b}}}(\kappa). \end{aligned} \tag{39}$$

In this framework, by increasing the number of Starlink LEO SVs the number of unknowns remains constant, i.e., only the rover position vector and the difference between the base and rover clock drift, which is defined as $\Delta\dot{t}_{r,b} \triangleq c(\delta\dot{t}_r - \delta\dot{t}_b)$ should be estimated. It should be noted that the success of the differential Doppler positioning method is dependent on the capability of a receiver in resolving the Doppler difference between the base and rover. Next, using the weighted nonlinear least square (WNLS) method, one searches for the solution to the following parameter vector $\boldsymbol{x} \triangleq \left[\boldsymbol{r}_r^{\mathsf{T}}, \Delta\dot{t}_{r,b}\right]^{\mathsf{T}}$. Let $\tilde{\boldsymbol{z}}$ denote the vector of all the pseudorange observables stacked together, and let $\boldsymbol{v}_{\tilde{z}}$ denote the vector of all measurement noises stacked together, which is a zero-mean Gaussian random vector with a diagonal covariance $\mathbf{R}(\kappa)$ whose diagonal elements are given by $\sigma_i^2(\kappa) = \sigma_{i_r}^2(\kappa) + \sigma_{i_b}^2(\kappa)$. Then, one can readily write the measurement equation given by $\boldsymbol{z} = \boldsymbol{g}(\boldsymbol{x}) + \boldsymbol{v}_z$, where $\boldsymbol{g}(\boldsymbol{x})$ is a vector-valued function that maps the parameter $\boldsymbol{x}$ to the pseudorange rate observables according to (38). An iterative Batched WNLS estimator with weight matrix $\mathbf{R}^{-1}(\kappa)$ is implemented to obtain an estimate of $\boldsymbol{x}$, denoted by $\hat{\boldsymbol{x}}$.

6. Experimental Results

This section presents experimental results of differential Doppler positioning with signals from unknown Starlink LEO SVs via the proposed framework. Two baselines between the base and the rover are considered: a far baseline of around 1 km and a close baseline of around 9 m. In what follows, the experimental setup is first discussed. Next, results from the acquisition and tracking stages of the Starlink receivers are demonstrated. Finally, receiver differential Doppler positioning results are presented for both baselines.

Experimental Setup

To demonstrate the performance of the proposed method, a stationary scenario is considered in which the base was equipped with an Ettus E312 universal software radio peripheral (USRP) with a consumer-grade Ku antenna and low-noise block (LNB) downconverter to receive Starlink signals in the Ku band, and the rover was equipped with USRP 2974 with the same downconverter. An Octoclock was used to synchronize between the clocks of the USRPs and the downconverters at the base and the rover. The sampling rate was set to 2.5 MHz, and the carrier frequency was set to 11.325 GHz, which is one of the Starlink downlink frequencies. The samples of the received signals were stored for off-line post-processing. The experimental setup is shown in Fig. 1.

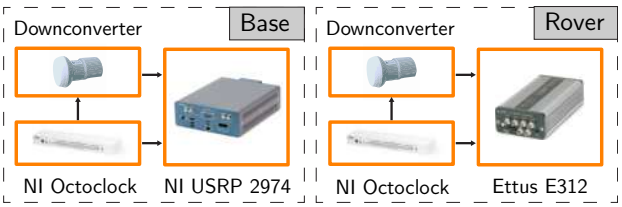

Figure 1. Base/rover experimental setup of the differential Doppler Starlink positioning framework.

Acquisition, Tracking, and Positioning Results

To evaluate the performance of the proposed differential Doppler positioning framework, two baselines between the base and rover are considered, namely 1.004 km and 8.65 m. The ground truth with which the position estimate was compared was taken from the navigation solution produced by the USRP's on-board GPS receiver.

Case 1: Base-Rover Baseline of 1.004 km

Over the course of the experiment, the receivers on-board the base and the rover were listening to three Starlink LEO SVs, namely Starlink 44740, 48295, and 47728. The satellites were visible for 320 seconds. Fig. 2 demonstrates the likelihood in terms of Doppler frequency and period for Starlink downlink signals. The CPI is considered to be 200 times the period. As can be seen from this figure, three Starlink LEO SVs were detected in the acquisition stage. The acquisition stage provides an initial value for the Doppler and the period of the downlink Starlink signals. The estimated Doppler and the Doppler rate were used in the tracking algorithm. Fig. 3 demonstrates the Doppler tracking results. It can be seen that three Starlink LEO SVs are tracked and the tracked Doppler follows that of TLE+SGP4 calculations. Fig. 4 shows the measured differential Doppler for the three LEO SVs. The spike in the estimated differential Doppler is due to channel outage and burst error, which is common in satellite communications.

The rover's initial position estimate was set to be approximately 200 km away from the base. The rover's position was estimated via the differential Doppler positioning framework described in Section 5. Fig. 5 shows that after six iterations, the 10^{-8} stopping criterion of the iterative WNLS algorithm was achieved. The 3–D position error was found to be 33.4 m. Upon equipping the receiver with an altimeter (to measure its altitude), the 2–D position error reduced to 5.6 m. Fig. 6 summarizes the positioning results.

Case 2: Base-Rover Baseline of 8.65 m

Similar to the previous case, over the course of this experiment, the receivers on-board the base and the rover were listening to three Starlink LEO SVs, namely Starlink 48466, 48295, and 45582. The satellites were visible for 600 seconds. The three Starlink LEO SVs were detected in the acquisition stage, when the CPI was set to be 200 times the period. The acquisition results were similar to those shown in Fig. 2. Fig. 7 demonstrates the Doppler tracking results. It can be seen that three Starlink LEO SVs are tracked and the tracked Doppler follows that of TLE+SGP4 calculations. Fig. 8 shows the measured differential Doppler for the three LEO SVs. It can be seen that the measured Doppler difference follows closely the predicted Doppler difference from TLE+SGP4 calculations.

The rover's initial position estimate was set to be approximately 12 km away from the base. The rover's position was estimated through the differential Doppler positioning framework described in Section 5. Fig. 9 shows that after four iterations, the 10^{-8} stopping criterion of the iterative WNLS algorithm was achieved. The 3–D position error was found to be 2.63 m. Upon equipping the receiver with an altimeter (to measure its altitude), the 2–D position error reduced to 2.56 m. Fig. 10 summarizes the positioning results.

7. Conclusion

This paper presented a framework that enabled achieving the first results of differential Doppler positioning with unknown Starlink LEO satellites. A sequential algorithm was proposed to estimate the number of active Starlink LEO SV signals and their corresponding RSs. It was shown that the classic linear model results in a so-called matched subspace detector. A closed-form of the probability of false alarm in the presence of Doppler estimation error was derived. A Doppler tracking algorithm was designed, which is based on the GLR detector. In order to capture the high dynamics of Starlink LEO SVs,

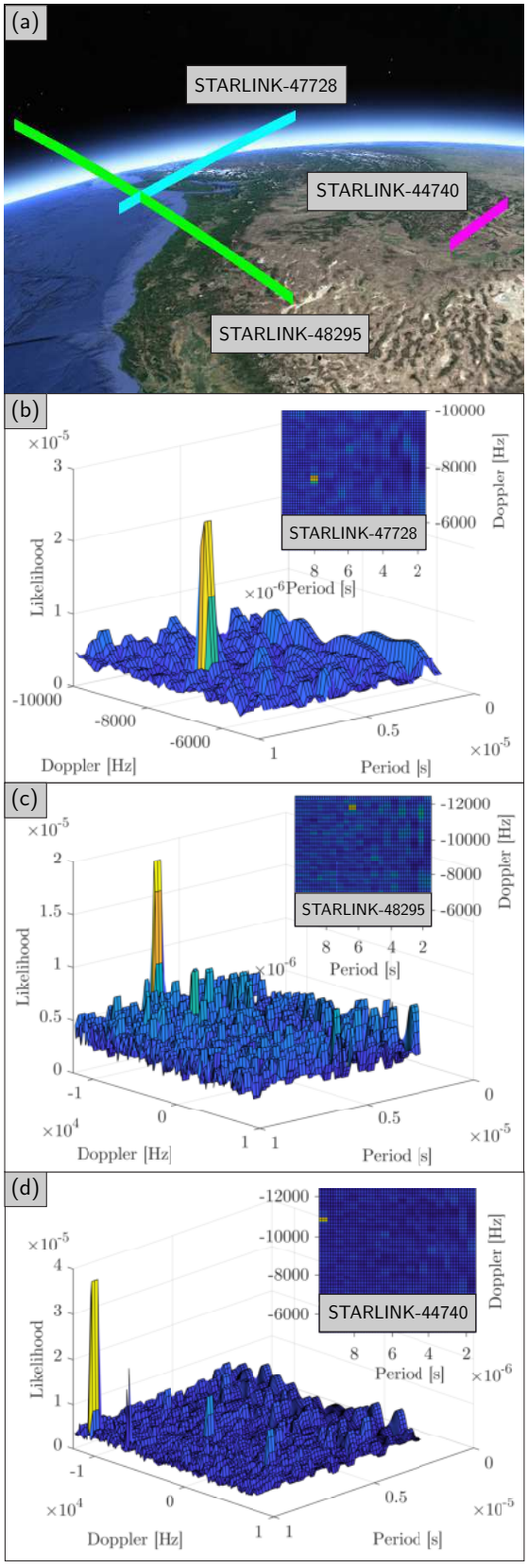

Figure 2. (a) Starlink LEO SVs' trajectories and (b)–(d) Acquisition of the three Starlink LEO SVs.

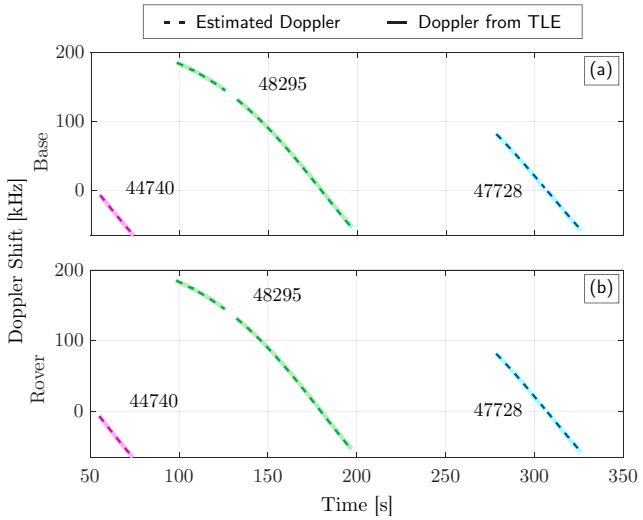

Figure 3. Doppler tracking of the three Starlink LEO SVs at the base and the rover compared with the TLE-based calculated Doppler.

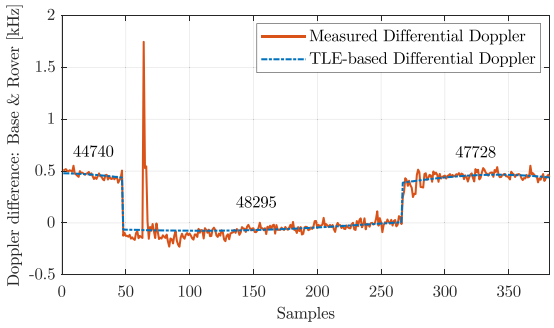

Figure 4. Measured Doppler difference between the base and the rover versus the predicted Doppler difference between between the base and the rover based on TLE+SGP4 calculations.

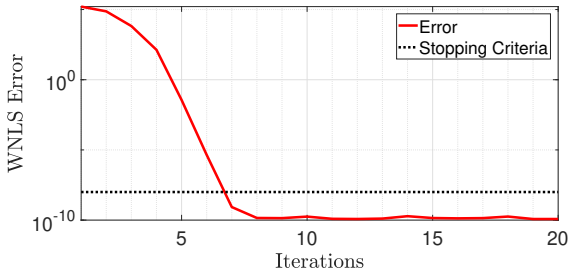

Figure 5. Iterative WNLS algorithm residual error.

in the Doppler tracking algorithm, a *linear chirp* model was considered, and a KF-based tacking algorithm was presented to track the chirp parameters. Experimental results evaluating the efficacy of the proposed framework were presented with two baselines (1 km and 9 m) between the base and rover receivers. Despite the fact that the satellites' ephemerides are poorly known (with errors on the order of several kilometersm since they are predicted from two-line element (TLE) files and an SGP4 propagator), the proposed differential framework was able to estimate the rover's two-dimensional position with an error of 5.6 m and 2.6 m, respectively.

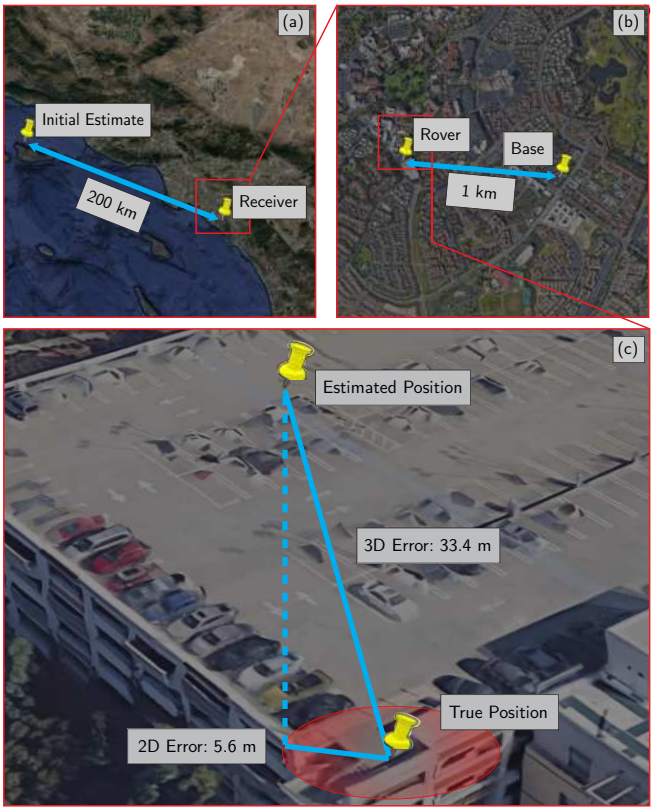

Figure 6. (a) Rover's initial position estimate, (b) Base's and rover's position, and (c) Rover's true and estimated position.

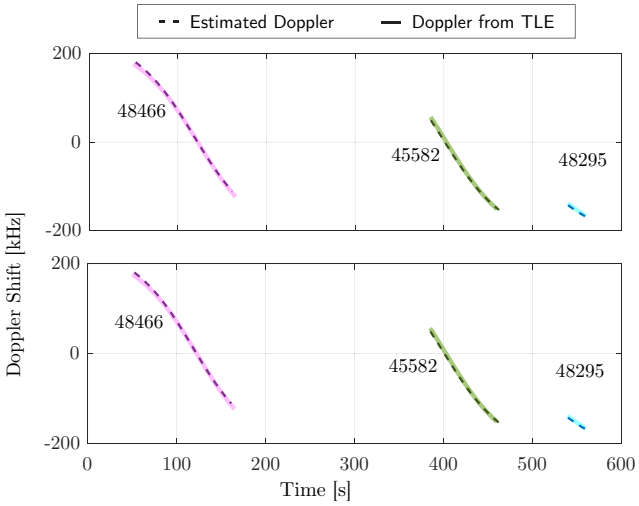

Figure 7. Doppler tracking of the three Starlink LEO SVs at the base and the rover compared with the TLE-based calculated Doppler.

APPENDICES

A. PROOF OF THEOREM 1

Given $\mathcal{W}_i$, for the general linear detection model (13), the GLR is derived as [70, Section 9.4.3]

$$\mathcal{L}(\mathbf{y}) = \frac{\left(\mathbf{A}\hat{\boldsymbol{\theta}}\right)^{\mathsf{H}} \left(\mathbf{A}\left(\mathbf{B}_i^{\mathsf{H}}\mathbf{B}_i\right)^{-1}\mathbf{A}^{\mathsf{H}}\right)^{-1} \left(\mathbf{A}\hat{\boldsymbol{\theta}}\right)}{\mathbf{y}\left(\mathbf{I}_L - \mathbf{B}_i\left(\mathbf{B}_i^{\mathsf{H}}\mathbf{B}_i\right)^{-1}\mathbf{B}_i^{H}\right)}, \quad (40)$$

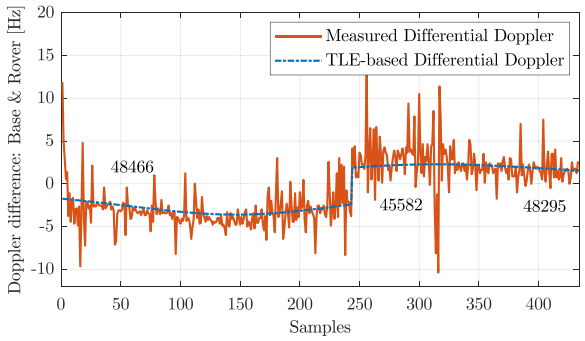

Figure 8. Measured Doppler difference between the base and the rover versus the predicted Doppler difference between between the base and the rover based on TLE+SGP4 calculations.

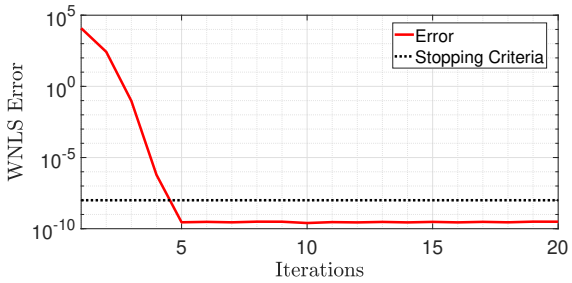

Figure 9. Iterative WNLS algorithm residual error.

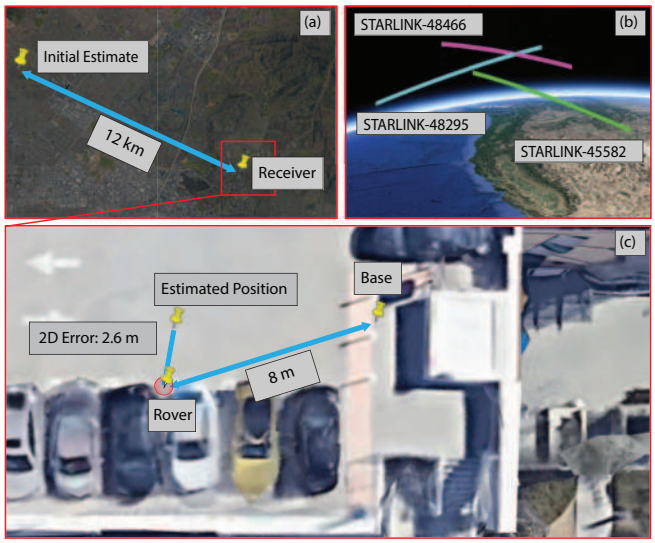

Figure 10. (a) Rover's initial position estimate, (b) Starlink LEO SVs' trajectories, and (c) Base's position and rover's true and estimated position.

Since, $\mathbf{y} = \mathbf{H}_i\mathbf{s}_i + \mathbf{B}_{i-1}\boldsymbol{\theta}_{i-1} + \mathbf{w}_{\mathrm{eq}_i}$, the least squares estimation of $\mathbf{s}_i$ is denoted by

$$\hat{\mathbf{s}}_i = \mathbf{J}_i^{-1}\mathbf{H}_i^{\mathsf{H}}\mathbf{P}^{\perp}_{\mathbf{B}_{i-1}}\mathbf{y}. \tag{41}$$

where $\mathbf{J}_i = \left(\mathbf{H}_i^{\mathsf{H}}\mathbf{P}^{\perp}_{\mathbf{B}_{i-1}}\mathbf{H}_i\right)$. Also, $\mathbf{P}_{\mathbf{X}} \triangleq \mathbf{X}(\mathbf{X}^{\mathsf{H}}\mathbf{X})^{-1}\mathbf{X}^{\mathsf{H}}$, denotes the projection matrix to the column space of $\mathbf{X}$, and

$$\mathbf{P}^{\perp}_{\mathbf{X}} \triangleq \mathbf{I}_L - \mathbf{X}\left(\mathbf{X}^{\mathsf{H}}\mathbf{X}\right)\mathbf{X}^{\mathsf{H}}, \tag{42}$$

denotes the projection matrix onto the space orthogonal to the column space of $\mathbf{X}$.

Using the matrix inversion lemma, one can show that

$$\left(\mathbf{B}_i^{\mathsf{H}}\mathbf{B}_i\right)^{-1} = \begin{bmatrix} \mathbf{Q}_1 & \mathbf{Q}_2 \\ \mathbf{Q}_3 & \mathbf{Q}_4 \end{bmatrix}, \tag{43}$$

where,

$$\mathbf{Q}_1 = \mathbf{J}_i^{-1},$$
$$\mathbf{Q}_2 = \left(\mathbf{H}_i^{\dagger}\mathbf{P}^{\perp}_{\mathbf{B}_{i-1}} - \mathbf{J}_i^{-1}\mathbf{H}_i^{\mathsf{T}}\right)(\mathbf{B}_{i-1}^{\dagger})^{\mathsf{H}},$$
$$\mathbf{Q}_3 = \mathbf{Q}_2^{\mathsf{H}},$$

and

$$\mathbf{Q}_4 = \mathbf{B}_{i-1}^{\dagger}\left(\mathbf{I}_L + \mathbf{H}_i\mathbf{J}_i^{-1}\mathbf{H}_i^{\mathsf{H}}\right)\left(\mathbf{B}_{i-1}^{\dagger}\right)^{\mathsf{H}},$$

where $\mathbf{H}^{\dagger} \triangleq \left(\mathbf{H}^{\mathsf{H}}\mathbf{H}\right)^{-1}\mathbf{H}^{\mathsf{H}}$.

It should be pointed out that the observation vector can be written as $\mathbf{y} = \mathbf{B}_i\boldsymbol{\theta}_i + \mathbf{w}_{\mathrm{eq}_i}$. Hence, the least squares estimation is obtained as

$$\hat{\boldsymbol{\theta}} = \left(\mathbf{B}_i\mathbf{B}_i\right)^{-1}\mathbf{B}_i^{\mathsf{H}}\mathbf{y}. \tag{44}$$

In the numerator of (40), one has

$$\begin{aligned}\mathbf{A}_i\hat{\boldsymbol{\theta}}_i &= \mathbf{A}_i\begin{bmatrix} \mathbf{Q}_1 & \mathbf{Q}_2 \\ \mathbf{Q}_3 & \mathbf{Q}_4 \end{bmatrix}\mathbf{B}_i^{\mathsf{H}}\mathbf{y} \\ &= \left(\mathbf{Q}_1\mathbf{H}_i^{\mathsf{H}} + \mathbf{Q}_2\mathbf{B}_{i-1}\right)\mathbf{y} \\ &= \mathbf{J}_{i-1}^{-1}\mathbf{H}_i^{\mathsf{H}}\left(\mathbf{I}_L - \mathbf{P}_{\mathbf{B}_{i-1}}\right)\mathbf{y}.\end{aligned}$$

Therefore, using (41), one has

$$\mathbf{A}_i\hat{\boldsymbol{\theta}}_i = \hat{\mathbf{s}}_i. \tag{45}$$

Moreover, using (43), one has

$$\mathbf{B}_i\left(\mathbf{B}_i^{\mathsf{H}}\mathbf{B}_i\right)^{-1}\mathbf{B}_i^{\mathsf{H}} = \mathbf{I}_L - \mathbf{P}^{\perp}_{\mathbf{B}_{i-1}} + \mathbf{P}^{\perp}_{\mathbf{B}_{i-1}}\mathbf{H}_i\mathbf{J}_i^{-1}\mathbf{H}_i^{\mathsf{H}}\mathbf{P}^{\perp}_{\mathbf{B}_{i-1}}. \tag{46}$$

Replacing (45) and (46) in (40) yields

$$\mathcal{L}_i(\mathbf{y}|\mathcal{W}_i) = \frac{\mathbf{y}^{\mathsf{H}}\mathbf{P}_{\mathbf{S}_i}\mathbf{y}}{\mathbf{y}^{\mathsf{H}}\mathbf{P}^{\perp}_{\mathbf{B}_{i-1}}\mathbf{P}^{\perp}_{\mathbf{S}_i}\mathbf{P}^{\perp}_{\mathbf{B}_{i-1}}\mathbf{y}}. \tag{47}$$

The matrices $\mathbf{H}_i$ and $\mathbf{P}^{\perp}_{\mathbf{B}_{i-1}}$ can be written as

$$\mathbf{H}_i = \mathbf{h}_i \otimes \mathbf{I}_L, \quad \mathbf{P}^{\perp}_{\mathbf{B}_{i-1}} = \bar{\mathbf{P}}^{\perp}_{\mathbf{i-1}} \otimes \mathbf{I}_{\mathbf{L}}, \tag{48}$$

where, $\mathbf{h}_i \triangleq [1, \exp(j\omega_i L), \ldots, \exp(j\omega_i(K-1)L)]^{\mathsf{T}}$, $\bar{\mathbf{P}}^{\perp}_{\mathbf{i-1}} \triangleq \left(\mathbf{I_L} - \mathbf{B_{i-1}}\left(\mathbf{B}_{\mathbf{i-1}}^{\mathsf{H}}\mathbf{B_{i-1}}\right)\mathbf{B}_{\mathbf{i-1}}^{\mathsf{H}}\right)$, $\mathbf{B}_{i-1} \triangleq [\mathbf{h}_1, \ldots, \mathbf{h}_{i-1}]$, and $\otimes$ denotes the Kronecker product. Hence, one can write

$$\mathbf{H}_i^{\mathsf{H}}\mathbf{P}^{\perp}_{\mathbf{B}_{i-1}}\mathbf{H}_i = \left(\mathbf{h}_i^{\mathsf{H}}\bar{\mathbf{P}}^{\perp}_{\mathbf{i-1}}\mathbf{h_i}\right) \otimes \mathbf{I}_L. \tag{49}$$

The scalar $\mathbf{h}_i^{\mathsf{H}}\bar{\mathbf{P}}^{\perp}_{i-1}\mathbf{h}_i$ can be written as

$$\mathbf{h}_i^{\mathsf{H}}\bar{\mathbf{P}}^{\perp}_{\mathbf{i-1}}\mathbf{h_i} = \mathbf{c_{ii}} - \left[\mathbf{c_{i1}}, \ldots, \mathbf{c_{i(i-1)}}\right] \cdot \begin{bmatrix} c_{11} & c_{12} & \ldots & c_{1(i-1)} \\ c_{21} & c_{22} & \ldots & c_{2i} \\ \vdots & \ddots & \ddots & \vdots \\ c_{i1} & c_{i2} & \ldots & c_{(i-1)(i-1)} \end{bmatrix}^{-1} \begin{bmatrix} c_{1i} \\ c_{2i} \\ \vdots \\ c_{(i-1)i} \end{bmatrix}, \tag{50}$$

which is the Schur complement of $\mathbf{C_{i-1}}$ of matrix $\mathbf{C_i}$ where

$$\mathbf{C_i} = \begin{bmatrix} c_{11} & c_{12} & \dots & c_{1i} \\ c_{21} & c_{22} & \dots & c_{2i} \\ \vdots & \ddots & \ddots & \vdots \\ c_{i1} & c_{i2} & \dots & c_{ii} \end{bmatrix}, \tag{51}$$

with $c_{ij} \triangleq \sum_{k=0}^{K-1} \exp\left(j(\omega_j - \omega_i)Lk\right)$. Hence, the following equality holds

$$\mathbf{H}_i^{\mathsf{H}} \mathbf{P}^{\perp}_{\mathbf{B}_{i-1}} \mathbf{H}_i = \lambda_i \mathbf{I}_L, \tag{52}$$

where the scalar λ_i is the Schur complement of block $\mathbf{C_{i-1}}$. Consequently, the likelihood (14) at the ith stage can be simplified as

$$\frac{\|\lambda_i^{-1} \hat{\mathbf{H}}_i^{\mathsf{H}} \mathbf{P}^{\perp}_{\mathbf{B}_{i-1}} \mathbf{y}\|^2}{\|\mathbf{P}^{\perp}_{\mathbf{B}_{i-1}} \mathbf{y}\|^2 - \|\lambda_i^{-1} \hat{\mathbf{H}}_i^{\mathsf{H}} \mathbf{P}^{\perp}_{\hat{\mathbf{B}}_{i-1}} \mathbf{y}\|^2} \underset{\mathcal{H}_0^i}{\overset{\mathcal{H}_1^i}{\gtrless}} \eta_i. \tag{53}$$

where η_i is a predetermined threshold at the ith stage. It can be shown that the likelihood (53) is a monotonically increasing function of $\frac{\|\hat{\mathbf{H}}_i^{\mathsf{H}} \hat{\mathbf{P}}^{\perp}_{\hat{\mathbf{B}}_{i-1}} \mathbf{y}\|^2}{\|\hat{\mathbf{P}}^{\perp}_{\hat{\mathbf{B}}_{i-1}} \mathbf{y}\|^2} \underset{\mathcal{H}_0^i}{\overset{\mathcal{H}_1^i}{\gtrless}}$, hence the GLR detector can be written as

$$\mathcal{L}(\mathbf{y}|\mathcal{W}_i) = \frac{\|\hat{\mathbf{H}}_i^{\mathsf{H}} \mathbf{P}^{\perp}_{\hat{\mathbf{B}}_{i-1}} \mathbf{y}\|^2}{\|\mathbf{P}^{\perp}_{\mathbf{B}_{i-1}} \mathbf{y}\|^2} \underset{\mathcal{H}_0^i}{\overset{\mathcal{H}_1^i}{\gtrless}} \eta_i. \tag{54}$$

B. Proof of Theorem 2

To calculate the probability of false alarm, the asymptotic distributions of the numerator and the denominator of the likelihood in (14) are determined under the null hypothesis.

The likelihood can be written as

$$\mathcal{L}(\mathbf{y}) = \frac{N(\mathbf{y})}{D(\mathbf{y})}. \tag{55}$$

First, the asymptotic distribution of the numerator is derived. It will be shown that the numerator follows a chi-squared distribution. According to (11), under the null hypothesis of the second stage, i.e., $\mathcal{H}_0^2$, the received signal vector can be written as $\mathbf{y} = \mathbf{B}_1\boldsymbol{\theta}_1 + \mathbf{w}_{\mathrm{eq}_2}$, where in a scenario with two sources with Doppler frequencies ω_1 and ω_2 one has $\mathbf{B}_1 = \mathbf{H}_1$ and $\boldsymbol{\theta}_1 = \mathbf{s}_1$. Hence, replacing $\mathbf{y} = \mathbf{B}_1\boldsymbol{\theta}_1 + \mathbf{w}_{\mathrm{eq}_2}$ in the numerator of the likelihood (14) results in

$$\begin{aligned} N(\mathbf{y}) = {} & \mathbf{s}_1^{\mathsf{H}} \mathbf{H}_1^{\mathsf{H}} \hat{\mathbf{P}}_{\mathbf{S_2}} \mathbf{H}_1 \mathbf{s}_1 + \mathbf{w}_{\mathrm{eq}_2}^{\mathsf{H}} \hat{\mathbf{P}}_{\mathbf{S_2}} \mathbf{w}_{\mathrm{eq}_2} \\ & + 2\Re\left\{\mathbf{s}_1^{\mathsf{H}} \mathbf{H}_1^{\mathsf{H}} \hat{\mathbf{P}}_{\mathbf{S_2}} \mathbf{w}_{\mathrm{eq}_2}\right\}, \end{aligned} \tag{56}$$

where $\hat{\mathbf{P}}_{\mathbf{S_2}} \triangleq \hat{\mathbf{P}}^{\perp}_{\hat{\mathbf{H}}_1} \hat{\mathbf{H}}_2 \left(\hat{\mathbf{H}}_2^{\mathsf{H}} \hat{\mathbf{P}}^{\perp}_{\hat{\mathbf{H}}_1} \hat{\mathbf{H}}_2\right)^{-1} \hat{\mathbf{H}}_2^{\mathsf{H}} \hat{\mathbf{P}}^{\perp}_{\hat{\mathbf{H}}_1}$, and $\Re\{\cdot\}$ denotes the real-part. Since, for all values of $i \neq j$, one has $\mathbf{H}_i^{\mathsf{H}}\mathbf{H}_i = K\mathbf{I}_L$, and $\mathbf{H}_i^{\mathsf{H}}\mathbf{H}_j = \exp\left(j(\omega_j - \omega_i)(K-1)L/2\right) \frac{\sin\left(\frac{(\omega_j - \omega_i)KL}{2}\right)}{\sin\left(\frac{(\omega_j - \omega_i)L}{2}\right)} \mathbf{I}_L$, it can be shown that

$$\begin{aligned} \mathbf{s}_1^{\mathsf{H}} \mathbf{H}_1^{\mathsf{H}} \hat{\mathbf{P}}_{\mathbf{S_2}} \mathbf{H}_1 \mathbf{s}_1 = {} & \left| \mathcal{S}(\omega_1, \hat{\omega}_2) - \frac{\mathcal{S}(\omega_1, \hat{\omega}_1)\mathcal{S}(\hat{\omega}_1, \hat{\omega}_2)}{K} \right|^2 \\ & \times \frac{K}{K^2 - |\mathcal{S}(\hat{\omega}_1, \hat{\omega}_2)|^2} \mathbf{s}_1^{\mathsf{H}} \mathbf{s}_1, \end{aligned} \tag{57}$$

where $\mathcal{S}(\omega_1, \omega_2) \triangleq \frac{\sin\left(\frac{(\omega_1 - \omega_2)KL}{2}\right)}{\sin\left(\frac{(\omega_1 - \omega_2)L}{2}\right)}$. If the Doppler estimation error of ω_1, defined as $\Delta\omega_1 \triangleq \omega_1 - \hat{\omega}_1$, satisfies $|\Delta\omega_1 L| \ll \frac{1}{K}$, and the difference between the estimate of the Doppler frequencies of the second Starlink satellite and the 1st Starlink satellite satisfies $|\hat{\omega}_2 L - \hat{\omega}_1 L| > \frac{1}{K}$; then, the following limit holds

$$\begin{aligned} \lim_{K\to\infty} & \left| \mathcal{S}(\omega_1, \hat{\omega}_2) - \frac{\mathcal{S}(\omega_1, \hat{\omega}_1)\mathcal{S}(\hat{\omega}_1, \hat{\omega}_2)}{K} \right|^2 \\ & \times \frac{K}{K^2 - |\mathcal{S}(\hat{\omega}_1, \hat{\omega}_2)|^2} \mathbf{s}_1^{\mathsf{H}} \mathbf{s}_1 = 0. \end{aligned} \tag{58}$$

The last term on the right hand side of (56) is a random sequence with mean $\mathbb{E}\left\{\mathbf{s}_1^{\mathsf{H}} \mathbf{H}_1^{\mathsf{H}} \hat{\mathbf{P}}_{\mathbf{S_2}} \mathbf{w}_{\mathrm{eq}_2}\right\} = 0$ and variance $\sigma^2 \mathbf{s}_1^{\mathsf{H}} \mathbf{H}_1^{\mathsf{H}} \hat{\mathbf{P}}_{\mathbf{S_2}} \mathbf{H}_1 \mathbf{s}_1$, which according to (58), asymptotically tends to zero as $K \to \infty$. Therefore,

$$\lim_{K\to\infty} N(\mathbf{y}) = \mathbf{w}_{\mathrm{eq}_2}^{\mathsf{H}} \hat{\mathbf{P}}_{\mathbf{S_2}} \mathbf{w}_{\mathrm{eq}_2}, \tag{59}$$

with probability one. Using similar steps for the denominator of (14), denoted by $D(\mathbf{y})$, it can be shown that

$$\lim_{K\to\infty} D(\mathbf{y}) = \mathbf{w}_{\mathrm{eq}_2}^{\mathsf{H}} \left(\hat{\mathbf{P}}^{\perp}_{\mathbf{H}_1} - \hat{\mathbf{P}}_{\mathbf{S_2}}\right) \mathbf{w}_{\mathrm{eq}_2}, \tag{60}$$

with probability one. According to equation (2.29) in [70], since $\hat{\mathbf{P}}_{\mathbf{S_2}}$ and $\hat{\mathbf{P}}_{\mathbf{H}_1}$ are idempotent matrices, $\frac{N(\mathbf{y})}{\sigma_w^2} \sim \chi^2_{2L}$, and $\frac{D(\mathbf{y})}{\sigma_w^2} \sim \chi^2_{2(KL-L)}$ as $K \to \infty$. Hence, utilizing to (9.15) in [70], the probability of false alarm equals

$$P_{\mathrm{fa}_i} = \exp\left(-L\eta_i\right) \sum_{n=0}^{L-1} \frac{(L\eta_i)^n}{n!}. \tag{61}$$

Acknowledgements

This work was supported in part by the Office of Naval Research (ONR) under Grant N00014-19-1-2511, in part by the Air Force Office of Scientific Research (AFOSR) under the Young Investigator Program (YIP) award, and in part by the U.S. Department of Transportation (USDOT) under Grant 69A3552047138 for the CARMEN University Transportation Center (UTC).

References

[1] T. Reid, K. Gunning, A. Perkins, S. Lo, and T. Walter, "Going back for the future: Large/mega LEO constellations for navigation," in *Proceedings of ION GNSS Conference*, September 2019, pp. 2452–2468.

[2] T. Reid, B. Chan, A. Goel, K. Gunning, B. Manning, J. Martin, A. Neish, A. Perkins, and P. Tarantino, "Satellite navigation for the age of autonomy," in *Proceedings of IEEE/ION Position, Location and Navigation Symposium*, 2020, pp. 342–352.

[3] D. Lawrence, H. Cobb, G. Gutt, M. OConnor, T. Reid, T. Walter, and D. Whelan, "Navigation from LEO: Current capability and future promise," *GPS World Magazine*, vol. 28, no. 7, pp. 42–48, July 2017.

[4] D. Racelis, B. Pervan, and M. Joerger, "Fault-free integrity analysis of mega-constellation-augmented GNSS," in *Proceedings of ION GNSS Conference*, January 2019, pp. 465–484.

[5] Z. Kassas, J. Morales, and J. Khalife, "New-age satellite-based navigation – STAN: simultaneous tracking and navigation with LEO satellite signals," *Inside GNSS Magazine*, vol. 14, no. 4, pp. 56–65, 2019.

[6] B. Li, H. Ge, M. Ge, L. Nie, Y. Shen, and H. Schuh, "LEO enhanced global navigation satellite system (LeGNSS) for real-time precise positioning services," *Advances in Space Research*, vol. 63, no. 1, pp. 73–93, 2019.

[7] Z. Kassas, J. Khalife, M. Neinavaie, and T. Mortlock, "Opportunity comes knocking: overcoming GPS vulnerabilities with other satellites' signals," *Inside Unmanned Systems Magazine*, pp. 30–35, June/July 2020.

[8] R. Morales-Ferre, E. Lohan, G. Falco, and E. Falletti, "GDOP-based analysis of suitability of LEO constellations for future satellite-based positioning," in *Proceedings of IEEE International Conference on Wireless for Space and Extreme Environments*, 2020, pp. 147–152.

[9] Q. Wei, X. Chen, and Y. Zhan, "Exploring implicit pilots for precise estimation of LEO satellite downlink doppler frequency," *IEEE Communications Letters*, vol. 24, no. 10, pp. 2270–2274, 2020.

[10] A. Nardin, F. Dovis, and J. Fraire, "Empowering the tracking performance of LEO-based positioning by means of meta-signals," *IEEE Journal of Radio Frequency Identification*, pp. 1–1, 2021.

[11] Z. Kassas, M. Neinavaie, J. Khalife, N. Khairallah, J. Haidar-Ahmad, S. Kozhaya, and Z. Shadram, "Enter LEO on the GNSS stage: Navigation with Starlink satellites," *Inside GNSS Magazine*, vol. 16, no. 6, pp. 42–51, 2021.

[12] T. Reid, A. Neish, T. Walter, and P. Enge, "Leveraging commercial broadband LEO constellations for navigating," in *Proceedings of ION GNSS Conference*, September 2016, pp. 2300–2314.

[13] T. Reid, A. Neish, T. Walter, and P. Enge, "Broadband LEO constellations for navigation," *NAVIGATION, Journal of the Institute of Navigation*, vol. 65, no. 2, pp. 205–220, 2018.

[14] Q. Wang, Z. Guo, Z. Sun, X. Cui, and K. Liu, "Research on the forward and reverse calculation based on the adaptive zero-velocity interval adjustment for the foot-mounted inertial pedestrian-positioning system," *Sensors*, vol. 18, no. 5, p. 1642, 2018.

[15] Y. Meng, L. Bian, L. Han, W. Lei, T. Yan, M. He, and X. Li, "A global navigation augmentation system based on LEO communication constellation," in *Proceedings of European Navigation Conference*, May 2019, pp. 65–71.

[16] P. Iannucci and T. Humphreys, "Economical fused LEO GNSS," in *Proceedings of IEEE/ION Position, Location and Navigation Symposium*, 2020, pp. 426–443.

[17] J. Khalife and Z. Kassas, "Receiver design for Doppler positioning with LEO satellites," in *Proceedings of IEEE International Conference on Acoustics, Speech and Signal Processing*, May 2019, pp. 5506–5510.

[18] H. Benzerrouk, Q. Nguyen, F. Xiaoxing, A. Amrhar, A. Nebylov, and R. Landry, "Alternative PNT based on Iridium Next LEO satellites Doppler/INS integrated navigation system," in *Proceedings of Saint Petersburg International Conference on Integrated Navigation Systems*, May 2019, pp. 1–10.

[19] R. Landry, A. Nguyen, H. Rasaee, A. Amrhar, X. Fang, and H. Benzerrouk, "Iridium Next LEO satellites as an alternative PNT in GNSS denied environments–part 1," *Inside GNSS Magazine*, vol. 14, no. 3, pp. 56–64., May 2019.

[20] Z. Tan, H. Qin, L. Cong, and C. Zhao, "New method for positioning using IRIDIUM satellite signals of opportunity," *IEEE Access*, vol. 7, pp. 83 412–83 423, 2019.

[21] F. Farhangian and R. Landry, "Multi-constellation software-defined receiver for Doppler positioning with LEO satellites," *Sensors*, vol. 20, no. 20, pp. 5866–5883, October 2020.

[22] M. Orabi, J. Khalife, and Z. Kassas, "Opportunistic navigation with Doppler measurements from Iridium Next and Orbcomm LEO satellites," in *Proceedings of IEEE Aerospace Conference*, March 2021, pp. 1–9.

[23] T. Reid, T. Walter, P. Enge, D. Lawrence, H. Cobb, G. Gutt, M. O'Conner, and D. Whelan, "Position, navigation, and timing technologies in the 21st century," J. Morton, F. van Diggelen, J. Spilker, Jr., and B. Parkinson, Eds. Wiley-IEEE, 2021, vol. 2, ch. 43: Navigation from low Earth orbit – Part 1: Concept, Current Capability, and Future Promise, pp. 1359–1379.

[24] Z. Kassas, "Position, navigation, and timing technologies in the 21st century," J. Morton, F. van Diggelen, J. Spilker, Jr., and B. Parkinson, Eds. Wiley-IEEE, 2021, vol. 2, ch. 43: Navigation from low Earth orbit – Part 2: models, implementation, and performance, pp. 1381–1412.

[25] J. Khalife, M. Neinavaie, and Z. Kassas, "The first carrier phase tracking and positioning results with Starlink LEO satellite signals," *IEEE Transactions on Aerospace and Electronic Systems*, 2021, accepted.

[26] L. Schiff and A. Chockalingam, "Signal design and system operation of Globalstar TM versus IS-95 CDMA – Similarities and differences," *Wireless Networks*, vol. 6, no. 1, pp. 47–57, February 2000.

[27] J. Raquet *et al.*, "Position, navigation, and timing technologies in the 21st century," J. Morton, F. van Diggelen, J. Spilker, Jr., and B. Parkinson, Eds. Wiley-IEEE, 2021, vol. 2, Part D: Position, Navigation, and Timing Using Radio Signals-of-Opportunity, ch. 35–43, pp. 1115–1412.

[28] J. del Peral-Rosado, R. Raulefs, J. López-Salcedo, and G. Seco-Granados, "Survey of cellular mobile radio localization methods: From 1G to 5G," *IEEE Communications Surveys Tutorials*, vol. 20, no. 2, pp. 1124–1148, 2018.

[29] Z. Kassas, "Position, navigation, and timing technologies in the 21st century," J. Morton, F. van Diggelen, J. Spilker, Jr., and B. Parkinson, Eds. Wiley-IEEE, 2021, vol. 2, ch. 38: Navigation with Cellular Signals of Opportunity, pp. 1171–1223.

[30] J. Yang, X. Wang, M. Rahman, S. Park, H. Kim, and Y. Wu, "A new positioning system using DVB-T2 transmitter signature waveforms in single frequency networks," *IEEE Transactions on Broadcasting*, vol. 58, no. 3, pp. 347–359, September 2012.

[31] T. Hong, J. Sun, T. Jin, Y. Yi, and J. Qu, "Hybrid positioning with DTMB and LTE signals," in *Proceedings*

of International Wireless Communications and Mobile Computing, July 2021, pp. 303–307.

[32] J. McEllroy, "Navigation using signals of opportunity in the AM transmission band," Master's thesis, Air Force Institute of Technology, Wright-Patterson Air Force Base, Ohio, USA, 2006.

[33] X. Chen, Q. Wei, F. Wang, Z. Jun, S. Wu, and A. Men, "Super-resolution time of arrival estimation for a symbiotic FM radio data system," *IEEE Transactions on Broadcasting*, vol. 66, no. 4, pp. 847–856, December 2020.

[34] R. Faragher and R. Harle, "Towards an efficient, intelligent, opportunistic smartphone indoor positioning system," *NAVIGATION, Journal of the Institute of Navigation*, vol. 62, no. 1, pp. 55–72, 2015.

[35] H. Zou, M. Jin, H. Jiang, L. Xie, and C. Spanos, "WinIPS: WiFi-based non-intrusive indoor positioning system with online radio map construction and adaptation," *IEEE Transactions on Wireless Communications*, vol. 16, no. 12, pp. 8118–8130, 2017.

[36] J. Khalife, M. Neinavaie, and Z. Kassas, "Navigation with differential carrier phase measurements from megaconstellation LEO satellites," in *Proceedings of IEEE/ION Position, Location, and Navigation Symposium*, April 2020, pp. 1393–1404.

[37] J. Haidar-Ahmad, S. Kozhaya, and Z. Kassas, "Comparison of neural network architectures for simultaneous tracking and navigation with LEO satellites," in *Proceedings of ION GNSS Conference*, September 2021, accepted.

[38] K. Shamaei and Z. Kassas, "A joint TOA and DOA acquisition and tracking approach for positioning with LTE signals," *IEEE Transactions on Signal Processing*, pp. 2689–2705, 2021.

[39] H. Dun, C. Tiberius, and G. Janssen, "Positioning in a multipath channel using OFDM signals with carrier phase tracking," *IEEE Access*, vol. 8, pp. 13 011–13 028, 2020.

[40] T. Kazaz, G. Janssen, J. Romme, and A. Van der Veen, "Delay estimation for ranging and localization using multiband channel state information," *IEEE Transactions on Wireless Communications*, pp. 1–16, September 2021.

[41] P. Wang and Y. Morton, "Multipath estimating delay lock loop for LTE signal TOA estimation in indoor and urban environments," *IEEE Transactions on Wireless Communications*, vol. 19, no. 8, pp. 5518–5530, 2020.

[42] P. Wang and Y. Morton, "Performance comparison of time-of-arrival estimation techniques for LTE signals in realistic multipath propagation channels," *NAVIGATION, Journal of the Institute of Navigation*, vol. 67, no. 4, pp. 691–712, December 2020.

[43] K. Shamaei and Z. Kassas, "Receiver design and time of arrival estimation for opportunistic localization with 5G signals," *IEEE Transactions on Wireless Communications*, vol. 20, no. 7, pp. 4716–4731, 2021.

[44] K. Shamaei and Z. Kassas, "Sub-meter accurate UAV navigation and cycle slip detection with LTE carrier phase," in *Proceedings of ION GNSS Conference*, September 2019, pp. 2469–2479.

[45] A. Abdallah and Z. Kassas, "UAV navigation with 5G carrier phase measurements," in *Proceedings of ION GNSS Conference*, September 2021, pp. 3294–3306.

[46] L. Scharf and B. Friedlander, "Matched subspace detectors," *IEEE Transactions on signal processing*, vol. 42, no. 8, pp. 2146–2157, 1994.

[47] S. Kraut, L. Scharf, and L. McWhorter, "Adaptive subspace detectors," *IEEE Transactions on Signal Processing*, vol. 49, no. 1, pp. 1–16, 2001.

[48] M. Korso, R. Boyer, A. Renaux, and S. Marcos, "Statistical resolution limit for source localization with clutter interference in a MIMO radar context," *IEEE Transactions on Signal Processing*, vol. 60, no. 2, pp. 987–992, 2012.

[49] A. Zaimbashi, M. Derakhtian, and A. Sheikhi, "GLRT-based CFAR detection in passive bistatic radar," *IEEE Transactions on Aerospace and Electronic Systems*, vol. 49, no. 1, pp. 134–159, 2013.

[50] I. Atitallah, A. Kammoun, M. Alouini, and T. Al-Naffouri, "Optimal design of large dimensional adaptive subspace detectors," *IEEE Transactions on Signal Processing*, vol. 64, no. 19, pp. 4922–4935, 2016.

[51] D. Ciuonzo, A. De Maio, and D. Orlando, "On the statistical invariance for adaptive radar detection in partially homogeneous disturbance plus structured interference," *IEEE Transactions on Signal Processing*, vol. 65, no. 5, pp. 1222–1234, 2017.

[52] A. Combernoux, F. Pascal, and G. Ginolhac, "Performance of the low-rank adaptive normalized matched filter test under a large dimension regime," *IEEE Transactions on Aerospace and Electronic Systems*, vol. 55, no. 1, pp. 459–468, 2019.

[53] Z. Wang, G. Li, and H. Chen, "Adaptive persymmetric subspace detectors in the partially homogeneous environment," *IEEE Transactions on Signal Processing*, vol. 68, pp. 5178–5187, 2020.

[54] M. Wax and A. Adler, "Detection of the number of signals by signal subspace matching," *IEEE Transactions on Signal Processing*, vol. 69, pp. 973–985, 2021.

[55] D. Roy, T. Mukherjee, M. Chatterjee, E. Blasch, and E. Pasiliao, "RFAL: adversarial learning for RF transmitter identification and classification," *IEEE Transactions on Cognitive Communications and Networking*, vol. 6, no. 2, pp. 783–801, 2019.

[56] M. Baek, S. Kwak, J. Jung, H. Kim, and D. Choi, "Implementation methodologies of deep learning-based signal detection for conventional MIMO transmitters," *IEEE Transactions on Broadcasting*, vol. 65, no. 3, pp. 636–642, 2019.

[57] G. Gao, "Towards navigation based on 120 satellites: Analyzing the new signals," Ph.D. dissertation, Stanford University, 2008.

[58] J. Merwe, S. Bartl, C. O'Driscoll, A. Rügamer, F. Förster, P. Berglez, A. Popugaev, and W. Felber, "GNSS sequence extraction and reuse for navigation," in *Proceedings of ION GNSS+ Conference*, 2020, pp. 2731–2747.

[59] M. Neinavaie, J. Khalife, and Z. Kassas, "Blind opportunistic navigation: Cognitive deciphering of partially known signals of opportunity," in *Proceedings of ION GNSS Conference*, September 2020, pp. 2748–2757.

[60] M. Neinavaie, J. Khalife, and Z. Kassas, "Blind Doppler tracking and beacon detection for opportunistic navigation with LEO satellite signals," in *Proceedings of IEEE Aerospace Conference*, March 2021, pp. 1–8.

[61] J. Khalife, M. Neinavaie, and Z. Kassas, "Blind Doppler tracking from OFDM signals transmitted by broadband LEO satellites," in *Proceedings of IEEE Vehicular Technology Conference*, April 2021, pp. 1–6.

[62] M. Neinavaie, J. Khalife, and Z. Kassas, "Cognitive opportunistic navigation in private networks with 5G signals and beyond," *IEEE Journal of Selected Topics in Signal Processing*, 2021, accepted.

[63] F. Gini and A. Farina, "Vector subspace detection in compound-Gaussian clutter. part I: survey and new results," *IEEE Transactions on Aerospace and Electronic Systems*, vol. 38, no. 4, pp. 1295–1311, 2002.

[64] M. Neinavaie, J. Khalife, and Z. Kassas, "Acquisition, doppler tracking, and positioning with Starlink LEO satellites: First results," *IEEE Transactions on Aerospace and Electronic Systems*, 2021, accepted.

[65] S. Kozhaya, J. Haidar-Ahmad, A. Abdallah, S. Saab, and Z. Kassas, "Comparison of neural network architectures for simultaneous tracking and navigation with LEO satellites," in *Proceedings of ION GNSS Conference*, September 2021, pp. 2507–2520.

[66] B. Parkinson and P. Enge, "Differential GPS," *Global Positioning System: Theory and applications.*, vol. 2, pp. 3–50, 1996.

[67] J. Rife, "Collaborative vision-integrated pseudorange error removal: Team-estimated differential GNSS corrections with no stationary reference receiver," *IEEE Transactions on Intelligent Transportation Systems*, vol. 13, no. 1, pp. 15–24, 2011.

[68] M. Rabinowitz, "A differential carrier-phase navigation system combining GPS with low Earth orbit satellites for rapid resolution of integer cycle ambiguities," Ph.D. dissertation, Stanford University, USA, 2000.

[69] T. Zhao and T. Huang, "Cramer-Rao lower bounds for the joint delay-Doppler estimation of an extended target," *IEEE Transactions on Signal Processing*, vol. 64, no. 6, pp. 1562–1573, 2016.

[70] S. Kay, *Fundamentals of statistical signal processing: Detection Theory*. Prentice-Hall, Upper Saddle River, NJ, 1993, vol. II.

[71] B. Tapley, B. Schutz, and G. Born, *Statistical Orbit Determination*. Burlington, MA: Elsevier Academic Press, 2004.

[72] J. Vetter, "Fifty years of orbit determination: Development of modern astrodynamics methods," *Johns Hopkins APL Technical Digest*, vol. 27, no. 3, pp. 239–252, November 2007.

[73] D. Vallado and P. Crawford, "SGP4 orbit determination," in *Proceedings of AIAA/AAS Astrodynamics Specialist Conference and Exhibit*, August 2008, pp. 6770–6799.

[74] J. Barnes, A. Chi, R. Andrew, L. Cutler, D. Healey, D. Leeson, T. McGunigal, J. Mullen, W. Smith, R. Sydnor, R. Vessot, and G. Winkler, "Characterization of frequency stability," *IEEE Transactions on Instrumentation and Measurement*, vol. 20, no. 2, pp. 105–120, May 1971.

BIOGRAPHY

Mohammad Neinavaie *is a Ph.D. student at the University of California, Irvine and a member of the Autonomous Systems Perception, Intelligence, and Navigation (ASPIN) Laboratory. He received an M.S. in digital communication systems from Shiraz University. His research interests include opportunistic navigation, cognitive radio, wireless communication systems, and software-defined radio.*

Zeinab Shadram *is a postdoctoral scholar at the University of California, Irvine and member of the ASPIN Laboratory. She received a B.S. and a M.S. in Aerospace Engineering from Sharif University of Technology (SUT) in Tehran, and a Ph.D. in mechanical and aerospace engineering from the University of California, Irvine. Her research interests include opportunistic navigation, wireless communication systems, and software-defined radio.*

Sharbel E. Kozhaya *is a Ph.D student in the Department of Electrical Engineering and Computer Science at the University of California, Irvine and a member of the ASPIN Laboratory. He received a B.E. in Electrical Engineering from LAU. His current research interests include opportunistic navigation, software-defined radio, low earth orbit satellites.*

Zaher (Zak) M. Kassas *is an associate professor at the University of California, Irvine and director of the Autonomous Systems Perception, Intelligence, and Navigation (ASPIN) Laboratory. He is also director of the U.S. Department of Transportation Center: CARMEN (Center for Automated Vehicle Research with Multimodal AssurEd Navigation), focusing on navigation resiliency and security of highly automated transportation systems. He received a B.E. in Electrical Engineering from the Lebanese American University, an M.S. in Electrical and Computer Engineering from The Ohio State University, and an M.S.E. in Aerospace Engineering and a Ph.D. in Electrical and Computer Engineering from The University of Texas at Austin. He is a recipient of the 2018 National Science Foundation (NSF) Faculty Early Career Development Program (CAREER) award, 2019 Office of Naval Research (ONR) Young Investigator Program (YIP) award, 2022 Air Force Office of Scientific Research (AFOSR) YIP award, 2018 IEEE Walter Fried Award, 2018 Institute of Navigation (ION) Samuel Burka Award, and 2019 ION Col. Thomas Thurlow Award. He is a Senior Editor of the IEEE Transactions on Intelligent Vehicles and an Associate Editor of the IEEE Transactions on Aerospace and Electronic Systems and the IEEE Transactions on Intelligent Transportation Systems. His research interests include cyber-physical systems, estimation theory, navigation systems, autonomous vehicles, and intelligent transportation systems.*